JAERI-M
8357

TWO-STAGE ACCELERATION OF AN ION BEAM FOR HIGH POWER ION SOURCE

July 1979

Yoshihiro OHARA

日本原子力研究所
Japan Atomic Energy Research Institute

この報告書は，日本原子力研究所がJAERI-Mレポートとして，不定期に刊行している研究報告書です．入手，複製などのお問合わせは，日本原子力研究所技術情報部（茨城県那珂郡東海村）あて，お申しこしください．

JAERI-M reports, issued irregularly, describe the results of research works carried out in JAERI. Inquiries about the availability of reports and their reproduction should be addressed to Division of Technical Information, Japan Atomic Energy Research Institute, Tokai-mura, Naka-gun, Ibaraki-ken, Japan.

JAERI-M 8357

Two-Stage Acceleration of an Ion Beam for High Power Ion Source

Yoshihiro OHARA

Division of Thermonuclear Fusion Research,
Tokai Research Establishment, JAERI

(Received July 6, 1979)

In research and development of a high power ion source for the JT-60 neutral beam injector, beam optics in the two-stage acceleration system has been investigated both numerically and experimentally. A computer code for cylindrically symmetric ion beam was developed for the simulation. By making use of this code, behaviour of the two-stage ion beam optics was clarified. The calculation results agreed well with the experimental ones. Experimentally, the gradient grid current and the grid heat loading proved to depend largely on the beam optics. The beam focusing by aperture displacement was investigated in thin lens approximation. The results obtained contributed to design and development of a high power ion source for the JT-60 neutral beam injector.

Keywords : JT-60 Tokamak, Neutral Beam Injector, Ion source, Two-Stage Acceleration, Two-Stage Beam Optics, Computer Simulation, Beam Focusing.

JAERI-M 8357

高出力イオン源のためのイオンビームの2段加速

日本原子力研究所東海研究所核融合研究部
小原　祥裕

（1979年7月6日 受理）

JT-60用中性粒子入射装置用高出力イオン源の開発研究の1つとして，2段加速系のビーム光学が計算機シミュレーション及び実験により調べられた。計算機シミュレーションのための，イオンビーム軌道計算コードが開発された。このコードを用いて，二段加速系のビーム光学が明らかになった。シミュレーションの結果は，実験結果とよい一致を示した。さらに，ビーム光学と電極熱負荷及び傾斜電極電流との深い関係が実験的に明確になった。一方，電極孔の軸ずれによるビーム集束法が，近軸近似により調べられた。得られた結果は，JT-60用中性粒子入射装置用高出力イオン源の設計及び開発に貢献した。

Contents

目　　次

§1. Introduction

In order to realize a reactor plasma, it is required not only to raize $n\tau$ above 10^{14} $cm^{-3}\cdot s$, but to increase the plasma temperature up to 10 keV. The Ohmic heating is not a promising tool for the attainment of reactor temperature. As one of the more powerful auxiliary heating methods, injection of powerful neutral beams is clearly expected.[1,2] The first injection experiments of neutral beams into tokamak plasma were performed at the Culham,[3,4] Princeton,[5] and Oak Ridge[6] Laboratories in 1972 - 1973 using the devices of CLEO, ATC, and ORMAK, respectively. The behaviour of the injected ions was found to be classical, and the expected plasma heating and D-D neutron production were observed. Since then, more powerful injection experiments on a number of tokamaks such as DITE,[7] TFR,[8] T-11,[9] and JFT-2[10] have been performed and resulted in bulk-ion heating without any deleterious effects on the plasma equilibrium or on the fast-ion slowing-down rate. Due to this favourable performance of neutral beam injection heating, and the continuing progress in the development of more powerful, higher-energy neutral beam injectors, we are convinced of attaining an ignition temperature in the future tokamaks such as TFTR, JET, T-20 or JT-60.[11] However, the development of high power and high energy ion source is one of the most difficult and important works for the powerful injectors. In the neutral beam injector for JT-60, the ion sources are required to deliver a low divergent hydrogen ion beam of 35 amp at 75 kV for 10 sec.[12] The e-folding gaussian beam divergence within

one degree at the ion current density above 0.27 amp/cm^2, are required to fit the acceptance angle of the tokamak device. However, the ion sources of these specifications have not been developed yet. Our efforts must be concentrated on beam optics, source plasma production and cooling of the extraction/acceleration grids which appear to be the basic problems involved in the high power and long duration ion source development. In particular, the improvement of beam optics is one of the most important and critical problems in designing an injector. In order to raize the injector efficiency, it is necessary to increase the beam power density or beam brightness. The beam power density is proportional to beam energy and beam current and decreases inversely as two powers of the beam divergence. Beam energy is determined by the thickness of tokamak plasma. Then, we must reduce the beam divergence at high current, in order to increase the beam power density. In general, however, the increase of beam divergence is inevitable with increasing beam current due to the space charge expansion. To overcome such behaviour of ion beam extraction, it is considered to decouple the current extraction stage and the acceleration stage, i.e., to employ a two-stage or a multiple stage acceleration system.

The purpose of this paper is to investigate the beam optics of two-stage electrostatic accelerator for high power and high energy ion source. Section 2 describes the relation of injection efficiency with the beamlet divergence and the focusing of individual beamlet to the injection port.

Section 3 describes the two-dimensional computer simulation code for ion beam trajectories, which was developed to design a extraction/acceleration system and the operation condition of an ion source. In section 4, two-stage beam optics is investigated both numerically and experimentally using a duopigatron plasma source with two-stage electrostatic accelerator. Section 5 describes the focusing of indivisual beamlet by aperture displacement in the two-stage acceleration system.

§2. Beamlet Divergence and Beam Focusing by Beamlet Steering

2.1 Introduction

Neutral beam injection heating experiments in many tokamaks have demonstrated that the injection of energetic neutral beams is one of the most effective and powerful methods for heating a tokamak plasma. In this method, it is required to extract a beam with low beam divergence to keep high injection efficiency against geometrical losses due to the long beam line and the injection port with limited area between the toroidal coils. This requirement becomes more important as the size of the torus becomes larger. The beam line is composed of neutralizer, pumping region, bending magnet and other required appliances including gate valve or beam dumper, and then the total injector length from the ion source to the injection port of the torus is up to several meters. Consequently, the extraction grid of the ion source is roughly regarded as a point source, when it is viewed from the injection port. In such a case, it is necessary to reduce the beamlet divergence as much as possible in order to raise the injector efficiency. However, it is not easy to obtain a beam with low beamlet divergence at high current density.

On the other hand, larger target plasma thickness demands further increase of beam energy, which induces a rapid decrease of neutralization efficiency above the beam energy around 60 keV. For the ion sources of JT-60 neutral

beam injector planned at the Japan Atomic Energy Research Institute, the proton beam accelerated to 75 kV is required, where the neutralization efficiency (power efficiency) is only 38 %.[12] In addition to the low neutralization efficiency, geometrical and reionization losses mean that the total injector efficiency amounts only to about 20 - 30 %. In view of the fact that neither the direct recovery of the energy of unneutralized ions nor the utilization of negative ions is developed yet, focusing the individual beamlets at the injection port appears to be a powerful and practical method for improving the injection efficiency. In particular, the importance of beam focusing may increase when we design an injector equipped with a few ion sources with a large extraction grid rather than many ion sources with a small extraction grid. In the following subsection, the improvement of injection efficiency by beam focusing is estimated quantitatively for a typical design of the future injector, in which we assume the beam intensity distribution function of each beamlet to be gaussian

2.2 Numerical Model of Beam Fraction to the Injection Port

We investigated numerically the effects of beam focusing on the fraction of beam passing through the injection port of the torus. In the numerical model, each beamlet has an axisymmetric gaussian beam intensity distribution with e-folding divergence ω.[13] Experimentally, the beam intensity distribution measured calorimetrically is almost gaussian.[14] The center of each beamlet extracted from the aperture at $Z = 0$ is directed toward a focal point at $Z = Z_f$. The radius of extraction grid at $Z = 0$ and that of the injection port at $Z = Z_p$ are denoted by R_g and R_p, respectively. The beam intensity I_i at the point (x,y) on the $Z = Z_p$ plane is expressed as follows when i-th beamlet is emitted from a point (X_g^i, Y_g^i) on the extraction grid (See Fig.2-1);

$$I_i = \left(\frac{1}{\pi R_o^2} \right) \exp \left\{ - \frac{R^2}{R_o^2} \right\} \qquad (2\text{-}1)$$

where

$$R_o = Z_p \tan \omega$$

$$R^2 = (X - X_p)^2 + (Y - Y_p)^2$$

$$X_p = \left(\frac{Z_p - Z_f}{Z_f} \right) \cdot X_g^i$$

$$Y_p = \left(\frac{Z_p - Z_f}{Z_f} \right) \cdot Y_g^i$$

Here, the point (X_p, Y_p) is the center of beamlet intensity

distribution at $Z = Z_p$. Consequently, the total fraction of the beam which pass through the injection port is obtained by the following equation;

$$F = \frac{1}{n} \iint \sum_{i=1}^{n} I_i \, dS$$

$$= \frac{1}{\pi n R_o^2} \iint \sum_{i=1}^{n} \exp \{ - \frac{R^2}{R_o^2} \} \, dS \qquad (2\text{-}2)$$

where n denotes the number of the beamlets in the extraction grid, and dS is the surface element in the injection port. When Z_f is infinite, we can obtain the beam fraction to the port without beam focusing. Using the above equation (2-2), we calculated the beam fraction through the injection port, where we neglected interception effect by the injector elements such as the beam limiter or neutralizer. A parameter survey was performed in the range of Z_p = 5 - 10 m, R_g = 6 ~ 18 cm and ω = 1.0° ~ 1.5° at R_p = 20 cm, which will cover typical design values of the injectors for future large tokamaks including JT-60.*)

---

*) In 1977, the design of JT-60 neutral beam injector was modified. The number of the ion sources stacked in each injector unit is reduced from four circular ion sources to two rectangular sources. The initial design values of R_g, R_p and Z_p are 6 cm, 20 cm, and 6.5 m, respectively.[15] In the modified design, the 12×27 cm rectangular extraction grid is adopted, and R_p and Z_p are 22 cm and 8.25 m, respectively.[12] The equivalent radius of the rectangular extraction grid R_g is approximately equal to 10 cm.

2.3 Computational Results

Figure 2-2 shows the dependence of the beam fraction passing through the injection port F on the distance between the extraction grid and the injection port Z_p, as a parameter of beamlet divergence. The broken curves indicate the case without beam focusing, and the solid curves indicate the case with beam focusing to the center of injection port. Here, the grid radius R_g and the port radius R_p are fixed to 6 cm and 20 cm, respectively. From this figure, we can see that the injection power decreases appreciably with Z_p, when Z_p becomes greater than several meters. However, we can improve the injection power by about several percent by the beam focusing, when Z_p is below 10 m. Figure 2-3 shows the relation between the beam fraction F and the beamlet divergence ω, when R_g = 6 cm, R_p = 20 cm and $Z_p = Z_f$ = 8 m. This result indicates the importance of reduction of beamlet divergence. We must necessarily obtain the low beamlet divergence below one degree, for the next stage injector.

Figure 2-4 shows the dependence of beam fraction F on Z_p as a parameter of grid radius R_g, where R_p and ω are fixed to 20 cm and 1.0° respectively. The solid line indicates the case with beam focusing to the injection port, and the injection efficiency decreases appreciably with Z_p, when Z_p becomes greater than several meters. The broken line indicates the case without beam focusing. From this figure, we can see that the effect of the beam focusing to raise the beam fraction passing through the injection port F is enhanced with the increase of grid radius. The beam focusing to the port is

not necessarily required when $R_g \lesssim 6$ cm. However, it is necessary to focus the beamlet axes to the port when R_g is greater than 10 cm. From the above numerical estimation, we can expect an improvement of injection efficiency of over 10 % using beam focusing in the present design of the JT-60 neutral beam injector. In addition, since the above results do not include the interception of the beam by appliances such as gas cell or beam limiters, beam focusing will become much more important when these intercepting obstacles exist. And so, effective focusing methods must be established for high power ion sources with a multiple-stage accelerator.

Beam deflection by grid misalignment may decrease the injection power appreciably. Grid misalignment about $\pm$ 0.1 mm is inevitable. Experiment[16] shows that the grid radial displacement of 0.1 mm makes the beam deflect by about 0.5 degrees. Figure 2-5 shows the influence of a beam deflection angle θ on F as a parameter of beamlet divergence ω, where R_g = 6 cm, R_p = 20 cm and $Z_p = Z_f$ = 8 m. The radial displacement of the beam center at $Z = Z_p$ is denoted by Δ. This result indicates that a deflection greater than about 0.5 degrees is sure to reduce the injection power considerably. Therefore, accurate beam steering to the center of the injection port is very important for an injector with small acceptance. An acceptable grid misalignment can be estimated in section 5.

§3. Computer Simulation Code of Ion Beam Trajectories

3.1 Simulation Model of Ion Beam Trajectories

A computer simulation code for cylindrically symmetric ion beams has been developed for the design of the ion extraction system and the optimum operating condition of an ion source.[17)]

Trajectories of ion beam are calculated by the equations of space-charge-limited current flow. The equations for space-charge-limited current are[18,19)]

Poisson's equation $$\nabla^2\phi = -\rho/\varepsilon_o \qquad (3\text{-}1)$$

Equation of motion $$m\frac{d\vec{v}}{dt} = e\vec{E} \qquad (3\text{-}2)$$

Equation of continuity $$\nabla\cdot\vec{J} = \nabla\cdot(\rho\vec{v}) = 0 \qquad (3\text{-}3)$$

where rationalized mks units are used and the notations have usual meanings. The magnetic field in the extraction region has bad effects on beam optics and produces separation of ion species, H_1^+, H_2^+, H_3^+, etc.. Therefore, the magnetic field free ion source is adopted for the present case. On the other hand, the magnetic field produced by ion beam itself is negligible. Hence the magnetic field is not taken into account in the equation (3-2). Under these conditions, it is easy to verify that beam trajectories don't depend on mass and electric charge. Historically, analytic solutions to these equations have been formulated by Langmuir and

Blodgett for plane parallel, coaxial cylindrical and coaxial spherical electrodes. More complicated geometries have proved intractable to analytic solution, but they can be solved by numerical methods.[20,21,22,23]

In the simulation model, the beam emitter surface is determined selfconsistently in such a way that the ion saturation current density is equal to that of the space-charge-limited current density. The potential of the emitter corresponds to that of the first electrode in contact with the source plasma. Finite ion and electron temperatures of the source plasma are taken into consideration as initial conditions of the beam trajectories. The ion starts from the emitter with an initial energy corresponds to about 3.5 times electron temperature T_e.[24] On the downstream side of the emitter, the electron density is far smaller than the ion density and is neglected in the code. The ion temperature T_i determines the initial direction of the emitting ion, which is obtained by the assumption of the drift-Maxwellian ion distribution at the emitter. The accelerated ions that pass through the zero equipotential surface under the grounded electrode do not suffer from space-charge-expansion because of the presence of electron cloud produced by the collisions of beam ions with the residual cold neutral gas. Therefore, the beam divergence is defined on this surface.

A block diagram of the digital computer program is shown in Fig.3-1. First, data are read in to define the dimensions of the problem, the electrode configuration, the electrode potentials, the total current and other parameters

needed for solution. The second acceleration region is divided into m(radially) × n(axially) meshes. Next, the Poisson's equation is solved to provide the potential distribution by means of successive over relaxation method. For the cylindrical coordinates, the finite difference equation at $R = r_0$ ($\neq 0$) is given by

$$b_1\phi_A + b_2\phi_B + b_3\phi_C + b_4\phi_D + b_5\phi_O = -\rho/\varepsilon_o \quad , \qquad (3\text{-}4)$$

where

$$b_1 = 2/a_1(1 + a_1)h_1^2$$

$$b_2 = (2r_0 + h_2) \; / \; r_0 a_2(1 + a_2)h_2^2$$

$$b_3 = 2 \; / \; (1 + a_1)h_1^2$$

$$b_4 = (2r_0 - a_2h_2) \; / \; r_0(1 + a_2)h_2^2$$

$$b_5 = -2 \; / \; a_1h_1^2 - 2 \; / \; a_2h_2^2 - (1 - a_2) \; / \; r_0a_2h_2 \quad .$$

On the axis, Eq.(3-4) is replaced by

$$b_1\phi_A + b_6\phi_B + b_3\phi_C + b_7\phi_D = -\rho/\varepsilon_o \quad , \qquad (3\text{-}5)$$

where

$$b_6 = 4 \; / \; a_2^2 \, h_2^2$$

$$b_7 = -2 \; / \; a_1h_1^2 - 4 \; / \; a_2^2 \, h_2^2 \quad .$$

ϕ_A, ϕ_B, ϕ_C, ϕ_D, ϕ_O are the potentials at points A, B, C, D

and O respectively; r_0, h_1, h_2, a_1, a_2 are defined in Fig.3-2. The electric field is obtained by linear interpolation of the mesh values. After the field distribution is obtained, beam trajectories are then calculated to provide a space charge distribution. The space charge density in the mesh ρ_{ij} is obtained by the following equation;

$$\rho_{ij} = \frac{1}{V_{ij}} \sum_m I^{(m)} t_{ij}^{(m)} \quad , \tag{3-6}$$

where V_{ij} is the volume of torus whose cross section is (i,j) cell, $I^{(m)}$ is the total current in the m-th beam and $t_{ij}^{(m)}$ is the time interval in which the m-th beam passes through the (i,j) cell. This is used in turn for a new solution of Poisson's equation followed by a re-computation of the trajectories. The calculation is thus repeated until the beam trajectories converge to a solution.

The program is checked by changing the potential, current density and dimensions in a fashion that keeps the perveance constant and then makes no difference in beam trajectories. The beam energy has some error below 1 ~ 2 percent because of the finite mesh approximation, but no significant change in the trajectories occurred compared with the analytical solution of a beam in field free space.

3.2 Validity of the Computer Code

In order to investigate the validity of this code, computed beam divergences (rms angle) are compared with the experimental data (1/e half widths) for the same configuration of the extraction electrodes as shown in Fig.3-3. Experimentally, beamlet characteristics have been measured with the help of the Faraday Cup placed 44 cm apart from the extraction electrodes, using a duopigatron ion source (See Fig.3-4). To match the computational results with the experimental data, it is important to assume that no ions are emitted from the peripheral region of the emitter, whose width λ corresponds approximately to the thickness of the wall sheath which is about ten times the Debye length of the source plasma.[24] This may be due to the fact that the ions in the wall sheath are mainly accelerated to the wall by the potential drop between the source plasma and the wall, and impinge on the wall before they are accelerated toward the downstream region.

Figure 3-5 shows the comparison of the beam divergence for proton beam, where the calculations are made under the condition of T_i = 1.1 eV, T_e = 10 eV and λ = 0.28 mm. Here, T_e can be determined by Langmuir probe experimentally and varies from several to 10 eV in our source plasma according to the operating condition. In the computation, however, the beam divergence does scarcely depend on T_e. On the other hand, T_i is not measured here, though the beam divergence increases with T_i in the computation. By choosing T_i to be around 2 eV, we can fit the data well. However, the above

calculations are made under the condition of T_i = 1.1 eV, according to some estimation about T_i.[22,25] This is mainly due to the fact that the computation model does not completely simulate the actual beam. Namely, the calculation does not include the mechanical error of the extraction electrodes, the density fluctuation of the source plasma, and the collisions in the ion acceleration region such as charge exchange and ionization. In addition, the influence of the stray magnetic field from the source magnet is not taken into consideration in the equation of motion. Due to these effects, the beam divergence measured will be greater by point several degree than that computed. This is why we chosen T_i to be 1.1 eV rather than to be about 2 eV. In the subsequent calculations, the parameters T_i, T_e and λ are chosen to be 1.1 eV, 10 eV and 0.28 mm, respectively.

On the other hand, the disagreement of the optimum perveance which gives the minimum beam divergence is mainly due to the fact that the calculation is made in the case of atomic hydrogen beam, while the actual beam consists of atomic and molecular ions. Now, we assume that the beam consists of H_1^+, H_2^+, and H_3^+ species in the ratio $\alpha:\beta:\gamma$ ($\alpha+\beta+\gamma = 1$), and the beam of mixed species is space-charge-limited. Then, the effective mass number of the mixed beam M_{eff} is given as follows,

$$M_{eff} = (\alpha + \sqrt{2}\,\beta + \sqrt{3}\,\gamma)^2 \quad . \tag{3-7}$$

Assuming that the beam trajectory does not vary in the case

of the mixed beam, the optimum perveance of the mixed beam P_{opt} is given by the next equation,

$$P_{opt} = P_{opt}(H_1^+) \times M_{eff}^{-1/2} \qquad (3\text{-}8)$$

where $P_{opt}(H_1^+)$ is the optimum perveance of proton beam. The typical beam composition of JAERI duopigatron is given as follows,[26]

$$\alpha : \beta : \gamma = 0.55 : 0.35 : 0.10$$

where the beam energy is 30 keV and the perveance is 4.9×10^{-9} pervs. In this case, $P_{opt} = 0.82 \times P_{opt}(H_1^+)$ and the ~20 % difference of optimum perveance between the experimental results and the calculation can be explained.

From the above points of view, we can conclude that the computer code simulates the actual ion beam trajectories not completely but fairly well.

§4. Two-Stage Acceleration of an Ion Beam

4.1 Introduction

The neutral beam injection turned out to be one of the most powerful and effective methods for heating a tokamak plasma. The neutral beam with tens of kilovolts energies is now achieved.[27,28,29,30] However, development of more powerful injectors are desired for the next generation tokamaks such as JFT, TFTR and JT-60. Moreover, larger target plasma thickness demonds the further increase of beam energy. For these tokamaks, the neutral beam injectors require the ion sources with beam energy of 50-150 keV, equivarent beam current of tens of amperes and divergence around one degree. However, in the case of single stage acceleration system, the beam power density inevitably decreases with the increase of acceleration energies above some level due to the electrical breackdown problems among extraction grids. This is because the ion current density is space-charge-limited and the breakdown distance for vacuum gaps is practically proportional to the square of an applied voltage.[31] Namely, the next relations hold,

$$I \propto V^{3/2}\, d^{-2} \tag{4-1}$$

$$V_b \propto d^{-1/2} \tag{4-2}$$

When the gap distance is chosen according to the breakdown distance, we obtain,

$$P_1 = V\ I = C\ V^{-3/2} \qquad (4\text{-}3)$$

where C is the constant. Then, the beam power density P_1 may decrease inversely as three-halves power of the acceleration voltage. This restriction is released by decoupling the current extraction stage and the acceleration stage, i.e., by employing a multiple stage acceleration system. If the extraction voltage V is divided into the first stage extraction voltage V_1 and the second stage acceleration voltage V_2 by adding one more grid, then the power density P_2 is given by the relation:

$$P_2 = C\ V_1^{-5/2}(V_1 + V_2) \quad . \qquad (4\text{-}4)$$

We find that the power density increases with the increase of the second stage acceleration voltage V_2, when the total acceleration voltage $V = V_1 + V_2$ is kept constant. Combining the Eq.(4-3) with Eq.(4-4), the ratio P_2/P_1 is given by

$$P_2/P_1 = (1 + V_2/V_1)^{5/2} \qquad (4\text{-}5)$$

From this relation, we can see that the two-stage acceleration system is more advantageous than the single stage system as the ratio V_2/V_1 increases. The above analysis is performed in the plane-parallel approximation. In fact, the beam power density (i.e. brightness) must be considered in the simultaneous constraint of beam optics. This is the reason why two-stage beam optics were investigated numerically by

the cylindrically symmetric two-dimensional ion beam code.

There are other advantages in the multi-stage acceleration system. By adopting the n-stage acceleration system, the breakdown distance becomes n-times smaller than that of the single stage when the total extraction voltage is constant. Therefore, this system reduces the collisions between beam ions and surrounding cold neutrals in the ion acceleration region. In a way it can be said that the voltage holding may be $\sqrt{n}$-times larger than that of the single stage if the gap distance is constant. As for the heat loading of the extraction grids, the heat loading W scales as follows according to Ref.(32),

$$W \propto n^{-7/4} \quad , \qquad (4\text{-}6)$$

Namely, the cooling problems of the extraction grids are reduced with the increase of the stage number n.

Consequently, the two-stage or multi-stage acceleration for neutral beam injectors has important meanings other than the convensional multi-stage electrostatic acceleration of high energy ion sources such as linac preinjector.

The requirements for the ion sources in the JT-60 injectors are as follows, where both initial design value and modified design value (shown in the branket) are presented:[12,15)]

Extraction Grid	: 12 cm diam.	(12 cm × 27 cm)
Transparency	: 40 %	(40 %)

Ion Species	: H_2	(H_2 or D_2)
Beam Energy	: 75 keV	(75 keV)
Beam Current	: 15 A	(35 A)
Current Density	: 330 mA/cm^2	(270 mA/cm^2)
1/e Divergence	: 1.0° ~ 1.2°	(1.0°)
Duration	: 5 ~ 10 sec	(10 sec)

In the modified design, further improvement in source plasma production is required, but the demand imposed on beam optics is somewhat relieved.

Here, we investigate numerically the optimum electrode geometries and operating conditions that satisfy the above requirements.

4.2 Electrode System of Two-Stage Acceleration

The two-stage acceleration system has four electrodes. The first stage is composed of the first and the second electrode, and the second stage is composed of the second, the third and the fourth electrode. Two models (Model A and Model B) have been investigated numerically, as to the two-stage acceleration systems. In the model A, (shown in Fig.4-1) the first electrode in contact with a source plasma is multi-aperture type and is held at the positive high potential corresponding to the desired beam energy. The second electrode is also multi-aperture type and spherically concave. The third electrode is a single disk aperture and is biased at negative potential to suppress the electron backstreaming from the subsequent beam-plasma region. The fourth electrode is also single aperture and is grounded electrically. The optimum configurations in the second stage have already been investigated numerically.[33,34] In the model B on the other hand, the first, the second, the third, and the fourth electrodes are all conventional multi-aperture type. In the following subsection, the optimum configurations in the model B are studied in detail.

There are many parameters in the extraction grids such as aperture diameter, gap distance, grid potential, grid thickness etc.. However, we investigate the effects of four characteristic parameters on the beam optics. They are aspect ratio $a = r_1/d_1$, gap ratio $g = d_1/d_2$, potential ratio $p = V_1/(V_2 + V_3)$, and the field intensity ratio $f = E_1/E_2 = p/g$. Here, r_1 is the radius of the first grid, d_1 and d_2 are the

first and the second gap distance, V_1, V_2+V_3, and V_3 are the potential drops in the first, the second and the third gap, and E_1 and E_2 are the electric field in the first and the second gap, respectively. As is shown in Fig.4-2, extraction grids form the positive-negative lens when f is smaller than unity and negative-negative lens when f is greater than unity.

4.3 Computer Simulation of Two-Stage Acceleration

4.3.1 Aperture Shape in the Plasma Grid

First, we examine the shape of aperture in the first positive grid. Figure 4-3 shows the dependence of the minimum beamlet divergence ω_{min} on the shape of aperture. Here, the minimum beamlet divergence is obtained by changing the ion saturation current density in the source plasma. In the case (a), the aperture is a disk type without chamfering of the edge. On the other hand, the edge of aperture is chamfered in the cases (b), (c), (d), (e), and (f). From this results, we see that the deeper chamfering of the edge reduces the beam divergence. However, when the chamfering is deeper above some level that is determined by the transparency of grids, the overlap of the chamfering between neighbouring ones is inevitable and consequently exercises bad influences on the beam optics. Therefore, we choose the shape in the case (e) for the subsequent calculations.

4.3.2 Single-Stage Acceleration

Secondly, we consider the single-stage extraction system composed of multi-aperture over the 12 cm diameter electrode with 40 % transparency. Putting the acceleration gap d is equal to the breakdown distance d_b, we calculate the minimum beamlet divergence and the total extraction current as a function of the aspect ratio. Assuming that all the beamlets have the same divergence, we do not distinguish hereafter the total beam divergence from the beamlet divergence, since we can focus all the beamlets on the focal point without changing the beamlet characteristics.

The breakdown distance d_b in vacuum has been investigated experimentally in some detail by the Culham group.[31] The group presented a relation $V = 60 \sqrt{d_b}$ (kV, cm) for the gap distance of 2-5.5 mm, while operating the source. Instead, we take somewhat artificially, the relation $d_b = (V/50)^2$ for the design limit of the gap distance. Since we assume that the potential of the positive and the negative electrodes are 75 kV and -2 kV, respectively, the gap distance is constant and is 2.37 cm. Therefore, Fig.4-4 can be regarded as indication of the relation between the beamlet divergence and the radius of the aperture. One may easily understand that it is quite difficult to reduce the beamlet divergence less than 0.75° if we need 75 keV proton beam, and that the beamlet divergence is larger than 1° for the total extraction current of 10 A.

4.3.3 Two-Stage Beam Optics

The dominant parameters in the two-stage acceleration system are the aspect ratio, gap ratio, potential ratio and the field intensity ratio as defined in the preceding subsection. Firstly, the parameter survey has been made by arbitrarily chosen several values of the aspect ratio and the gap ratio. Figure 4-5(a) shows the dependence of the beamlet minimum divergence ω_{min} on the field intensity ratio f, for the fixed acceleration voltage of 75 kV, where the breakdown limit for the gap distance is neglected. Although it does not cover enough ranges of the parameters,*) one finds that ω_{min} decreases almost proportionally with decreasing f, and does not depend strongly on the aspect ratio and the gap ratio if f is fixed.

We then take into account the breakdown limit for the gap distance using the scaling low of the ion beams. The beam optics is unchanged when the distance scale length is changed. Combination of the equation of motion, Equation of continuity, and Maxwell's equation lead us to the scaling law for the beamlet current and perveance.[18] Namely, if α and β are the scaling factors of the geometrical length and the applied potential respectively, then the beamlet current I scales as

$$I \rightarrow \beta^{3/2} I$$

For the fixed diameter and transparency of the extraction grids, the number of apertures n scales according to

*) Namely, the gap ratio g is chosen to be less than 1, and the product of a and g is small (less than 0.35).

$$n \rightarrow n/\alpha^2$$

Thus, the total extraction current I_{tot} and the total perveance P_{tot} scales according to

$$I_{tot} \rightarrow \beta^{3/2}\alpha^{-2} I_{tot}$$

$$P_{tot} \rightarrow \alpha^{-2} P_{tot}$$

Using the above relations, we scale the gap distance such that either d_1 or d_2 may coincide with the break down limit, while the other still satisfys the relation $d \geq (V/50)^2$. The transparency and the grid diameter are assumed to be the same as in the preceding subsection. Figure 4-5(b) shows the total current thus obtained. It should again be noted that it does not cover enough ranges of parameters. We only use this figure for the general parameter servey.

Above calculations lead us to the following relations, where the notations ↑, ↓ and ~ mean the increase, the decrease, the nearly equal respectively.

$$g\left(=\frac{d_1}{d_2}\right)\uparrow \quad \left\{\begin{array}{l} d_1 \uparrow \Rightarrow \left\{\begin{array}{l}\omega_{min}\downarrow \\ \text{and} \\ P_{opt}\downarrow\end{array}\right. \\ \text{or} \\ d_2 \downarrow \Rightarrow \left\{\begin{array}{l}\omega_{min}\downarrow \\ \text{and} \\ P_{opt}\uparrow\end{array}\right. \end{array}\right\} f\left(=\frac{p}{g}\right)\downarrow \Rightarrow \left\{\begin{array}{l}\omega_{min}\downarrow \\ \text{and} \\ P_{opt}\downarrow\uparrow\end{array}\right.$$

$$P\left(=\frac{V_1}{V_2+V_3}\right)\downarrow \quad \Rightarrow \quad \left\{\begin{array}{l}\omega_{min}\downarrow \\ \text{and} \\ P_{opt}\downarrow\end{array}\right.$$

$$a\left(=\frac{r_1}{d_1}\right)\downarrow \quad \left\{\begin{array}{l} r_1\downarrow \Rightarrow \left\{\begin{array}{l}\omega_{min}\sim \\ \text{and} \\ P_{opt}\downarrow,\ P_{tot}\uparrow\end{array}\right. \\ \text{or} \\ d_1\uparrow \Rightarrow \left\{\begin{array}{l}\omega_{min}\downarrow \\ \text{and} \\ P_{opt}\downarrow\end{array}\right.\end{array}\right.$$

Here, P_{opt} is the value of P where ω takes the minimum. Thus the appropriate way to decrease ω_{min} and to increase P_{opt} is to decrease d_2. The smaller d_1 gives the larger P_{opt}, but increases ω_{min} simultaneously. Although the smaller r_1 gives the smaller P_{opt}, the total perveance P_{tot} generally increases.

4.3.4 Optimization of Two-Stage Acceleration System

In order to obtain a high extraction current with small beam divergence, both d_1 and d_2 are minimized to the design limit. The design limit here is again chosen to be the breakdown distance $d_B = (V/50)^2$, (cm, kV). Solving a set of equations,

$$\begin{aligned} V_1 &= 50\sqrt{d_1} \\ V_2 + V_3 &= 50\sqrt{d_2} \\ V &= V_1 + V_2 \\ f &= \frac{V_1}{V_2 + V_3} \cdot \frac{d_2}{d_1} \end{aligned} \tag{4-7}$$

we obtain

$$\begin{aligned} V_1 &= \frac{V + V_3}{1 + f} \\ V_2 &= \frac{fV - V_3}{1 + f} \end{aligned} \tag{4-8}$$

and

$$\begin{aligned} d_1 &= \left[\frac{1}{50} \cdot \frac{V + V_3}{1 + f} \right]^2 \\ d_2 &= \left[\frac{1}{50} \cdot \frac{f(V + V_3)}{1 + f} \right]^2 = f^2 d_1 \end{aligned} \tag{4-9}$$

Thus, potential differences V_1 and V_2, and distances d_1 and d_2 are uniquely determined in terms of V, f and V_3.

From the designing point of view, there may be a minimum limit on the aperture diameter provided the transparency is kept constant. This is because the grid thickness or the size of the cooling pipe cannot scale too small. In this connection, we fix the aperture diameter around 3.5 mm. Figure 4-6 shows the dependence of ω_{min} and $P_{opt}(I_{opt})$ on the field intensity ratio for the proton beam accelerated from the 3.5 mm diam. aperture at V = 75 kV. The extraction electrodes are again 12 cm in diameter and have 40 % transparency. In order to extract total ion current of 15 A, f should be larger than 0.6, and the corresponding beamlet divergence ω_{min} is larger than 0.74°. The ion saturation current density J_{sat} required for the source plasma should be greater than 450 mA/cm^2. If f is chosen to be 0.6, and 0.8, potentials and grid distances are summarized in Table I. Figure 4-7 shows the beam trajectories calculated for typical values of f.

When the gap distances are determined by the equation $d = (V/40)^2$ instead of $d = (V/50)^2$, a larger safety factor is included against breakdowns but less currents are extracted from the same diam. grids (See Fig.4-8). In this case, the beamlet divergence becomes greater than 1.2°, if one tries to extract 15 A. Thus the critical gap distance as imposed on the grid design basis influences the beam property significantly. In this connection, a problem remains about to what ranges or in what conditions the Culham's empirical law can be extrapolated in the case of multi-stage extraction system. For instance, the critical distance may presumably

be influenced by the presence of working gas introduced into the grid region, or by the presence of impinging ions and/or secondary electrons on and from the aperture edges.

To improve the beam divergence, two approaches are considered. The one is to change the radius of the aperture, and the other is to increase the gap distance. In the preceding subsection, the gap distances are chosen to be equal to the breakdown limit. Here, we increase either d_1 or d_2 greater than the design limit.

Firstly, the aperture diameter is changed with other parameters remain unchanged. It is found that the beamlet divergence at the extraction of 15 A decreases with decreasing aperture diameter, although it saturates to decrease for the aperture radius less than 3.5 mm. The results are shown in Fig.4-9.

Secondly, the gap distance is increased such that either d_1 or d_2 becomes greater than the design limit. The parameter f decreases with increasing d_1, and increases with increasing d_2. The results are shown in Fig.4-10, where the beam divergence and the total current change appreciably when the gap distance is increased from the reference point denoted by the circles at f = 0.5, 0.8 and 1.2 (where the gap distances are minimized to the design limit). In consequence, the beam divergence is not improved and moreover, the extraction current decreases significantly.

Thus it may be recommended that the aperture diameter should be 3.0-3.5 mm and the gap distances be equal to the breakdown design limit.

4.3.5 Three-Stage Acceleration

In Fig.4-5, the minimum beam divergence decreases with decreasing field intensity ratio and is less than 0.5 degree for $f \leq 0.5$, although the extraction current is low. In Figs.4-6 ~ 4-9, however, the minimum beam divergences saturate to decrease with decreasing f. Here, we will investigate this discrepancy and try to improve the beam divergence without losing high extraction current. We find that the 2nd aspect ratio a_2, defined by the radius of the second stage acceleration aperture r_2 divided by the second gap d_2, is the important parameter. Namely, in Fig.4-5, a_2 (= a·g) is always less than 0.35, while in Figs.4-5 ~ 4-9, a_2 is much larger for small values of f.*) Indeed, the decrease of f is effective in reducing the beam divergence, provided the field intensity ratio represents the approximate value on the aperture axis. When a_2 is large, however, the electric field is strongly deformed near the aperture axis as shown in the latter half of Fig.4-7. Thus, even if f is less than 0.5, the value of f_{axis} (the field intensity ratio defined at the aperture axis) is much larger, and therefore the minimum beam divergences are not improved. To overcome this difficulty, two methods may be considered. The first one is to decrease the 2nd aspect ratio a_2 without changing other parameters. In order to achieve this situation, the aperture diameter of the 2nd positive and negative grids are decreased. The second way is to apply three-stage acceleration system by adding one more grid (the third positive grid) and to make thus combined 2nd and the 3rd

*) For instance, a_2 = 0.70, 0.95 and 1.46 corresponding to the latter three cases in Fig.4-7.

electric field approach uniform.

For the first way, we find that the minimum beam divergence can be reduced by 0.05° when $2r_2$ and $2r_3$ are decreased from 3.5 mm to 2.45 mm (a_2 : 1.39 → 0.97) for the case of f = 0.3. For the second way, the potential difference between grids V_i and the gap distance d_i are given by

$$V_1 = \frac{V + V_4}{1 + f_1 + f_1 f_2}$$

$$V_2 = \frac{f_1(V + V_4)}{1 + f_1 + f_1 f_2} \qquad (4\text{-}10)$$

$$V_3 = \frac{f_1 f_2 V - (1 + f_1)V_4}{1 + f_1 + f_1 f_2}$$

and

$$d_1 = (V_1/50)^2 \quad (\text{kV, cm})$$

$$d_2 = (V_2/50)^2 = f_1^2\, d_1 \qquad (4\text{-}11)$$

$$d_3 = (V_3 + V_4/50)^2 = f_1^2\, f_2^2\, d_1$$

where f_1 and f_2 are defined by

$$f_1 = \frac{E_1}{E_2} = \frac{V_1 d_2}{V_2 d_1}$$

$$f_2 = \frac{E_2}{E_3} = \frac{V_2 d_3}{(V_3 + V_4) d_2} \qquad (4\text{-}12)$$

We calculate next two cases assuming the aperture diameters

$$2r_1 = 2r_5 = 3.5 \text{ mm}, \quad 2r_2 = 2r_3 = 2r_4 = 2.45 \text{ mm} \quad .$$

(a) $f_1 = f_2 = 0.5$

(b) $f_1 = 0.37, \quad f_2 = 1.0$

Figure 4-11 shows the beam trajectories for the above cases. We find that the minimum beam divergence is reduced to 0.58° and 0.63° in the case (a) and (b), respectively. Thus the beam divergence is improved by about 0.1° by introducing the three stage acceleration system.

4.3.6 Conclusion

From our computational results, we find it possible to obtain a proton beam with energy of 75 keV, current of 15 A and divergence of about 0.6 degree from the 12 cm diam. extraction grids with 40 % transparency. In this computation, the effects of the ion and electron temperature of the source plasma on the beam optics are included. But, there are other factors which increase the total beam divergence. In the first place, the total beam is obtained through the extraction grids with hundreds of apertures, while the computation is carried out on the beamlet. Therefore, the aberration may be increased not only by mechanical error of the grids system but by deformation of the grids by heat loads. Due to these errors, some of the beamlets are also deflected and the injection power through the port may be reduced. Namely, the divergence increases effectively. In the second place, the divergence may be increased by the fluctuation and density gradient over the extraction grid in the source plasma. In the third place, although the actual beam is composed of atomic and molecular ions, the effects of mixed species on beam characteristics are not considered in the computation. Finally, the collisions such as charge exchange, ionization and desociation are not considered in the ion acceleration region. In addition, the ion backstream from the subsequent beam plasma region is not included in the calculation. These effects may change the beam optics as well as increase the heat load of the grids. Consequently, the divergence of the actual multiampere beam becomes larger

than that of the computation by about 0.2° - 0.3°.

The electrical breakdown among extraction grids has important effects on the beam characteristics. It is necessary to investigate the breakdown condition above tens of kilovolts, which may depend, for example, on the gas pressure between the grids and the materials of the grids.

It is found that the beam divergence in the two-stage configuration depends strongly on the field intensity ratio f, and the optimum value of f that gives the minimum beam divergence is about 0.3 - 0.5. It also depends on the second stage aspect ratio a_2, which in turn affects the field intensity ratio on the beamlet axis. The three-stage acceleration is superior to the two-stage in that the smaller field intensity ratio is easily obtained on the axis of the aperture when the gap distance is chosen according to the breakdown distance.

4.4 Experimental Results of Two-Stage Beam Optics

4.4.1 Experimental Procedure

The experiments were performed with a JAERI 7-cm duopigatron plasma source with two-stage acceleration system, which is shown in Fig.4-12. The two-stage acceleration system (Model B) is composed of four grids called plasma grid, gradient grid, suppressor grid and exit grid, respectively (See Fig.4-13). The plasma grid in contact with a source plasma is held at a positive high potential corresponding to the desired beam energy V_{tot} (= V_{ext} + V_{acc}). The potential V_{acc} is applied at the gradient grid. The suppressor grid is biased at negative voltage V_{dec} to suppress the electron backstreaming from the downstream beam plasma region. In the present experiments, V_{dec} is fixed to 1.6 kV. The exit grid is grounded electrically. The electric currents into the plasma, the gradient and the suppressor grid are denoted as I_p, I_g and I_{dec}, respectively. The polarity of the current I_g is also shown in Fig.4-13. The accel drain current is expressed as I_{acc}, and is equal to $I_p - I_g$. The extraction grids are made of 15 cm diam. copper disk with 83 apertures over central 5 cm diam. area. The aperture diameter is 3.5 mm in the plasma and the gradient grid, while it is 4.0 mm in the suppressor and the exit grid. The hole pattern is split into 5 sections by 6 water lines. The transparency of the grids is 43 %. The grid thickness is 2.0 mm in the plasma and the exit grid and 1.5 mm in the gradient and the suppressor grid. The extraction

and the acceleration gap distance denoted by d_{ext} and d_{acc}, respectively, are changed in the range of 4.5 - 8.0 mm. The decel gap distance is fixed to 2.5 mm in the present experiments.

The ion source is operated with a continuous hydrogen gas flow from the hot cathode region. The ion beam up to 2.0 A is extracted stably in the range of total acceleration energy 50 - 70 keV. The duty cycle of beam extraction is 1/10 - 1/30, and the beam pulse length is typically 100 milliseconds. The e-folding half-width beam divergence is measured by the scanning colorimeter set 1.0 m apart from the extractor. The beam dumper of 20 cm diam. is placed 1.6 m apart from the extractor.

To develop ion sources of these specifications, we have constructed a 100 kV test stand.[35] The two-stage series power supplies are capable of delivering ion beams up to 40 A at 100 kV level. The voltage up to 80 kV is regulated by the series tubes, EIMAC Y676 (for the accelerator P.S.), and Y546s (for the extractor and decelerator P.S.). They also serve to modulate the current in the case of breakdowns within 200 μsec. The system can provide the pulsed arc power either followed by the pulsed acceleration voltage, or under the continuous acceleration voltage.

4.4.2 Effects of Gas Pressure on Beam Optics

We first investigate the effect of operating gas pressure on beam optics to see the pressure range under which the beam optics is not influenced. Here, the beam divergences are measured as a function of hydrogen gas pressures both in the hot cathode region P_{fil} and in the beam flight region P_{vac}. Figure 4-14 shows the dependence of the beam divergence and I_{dec} on P_{vac}, where P_{vac} is changed by introducing the hydrogen gas to the beam flight region. Other parameters such as P_{fil}, V_{ext}, V_{acc} and I_{acc} are all fixed; P_{fil} = 0.07 Torr, V_{ext} = 15 kV, V_{acc} = 35 kV and I_{acc} = 0.6 A. This figure indicates that the beam divergence is scarcely influenced by the pressure P_{vac} when P_{vac} ranges from 2×10^{-4} Torr to 1×10^{-3} Torr. However, a slight increase of the beam divergence is observed above the pressure 1×10^{-3} Torr. This is mainly due to the increase of angular scattering of beam ions with surrounding cold neutrals. On the other hand, I_{dec} increases rapidly above the pressure 1×10^{-3} Torr, followed by the considerable increase of x-ray radiation from the ion source. This may be due to the increase of ion backstreaming from the beam plasma.

Figure 4-15 shows the relation between P_{fil} and the beam divergence, where $P_{vac} = 3 \times 10^{-4}$ Torr, V_{ext} = 15 kV, V_{acc} = 35 kV and I_{acc} = 0.6 A. The pressure P_{fil} is changed by controlling the gas flow rate supplied to the hot cathode region of the ion source. Simultaneously, it is necessary to change the arc current to keep the drain current I_{acc} constant. The arc current I_{arc} required, and the decel

current I_{dec} are also shown in the same Figure. From this result, one finds that the beam divergence is not influenced by P_{fil} in the range of P_{fil} = 0.05 - 0.15 Torr. Furthermore, when P_{fil} is smaller than about 0.05 Torr, the source plasma becomes noisy. However, we can't observe the bad effect of the density fluctuation on beam divergences. On the other hand, the increase of P_{fil} also raises the gas pressure in the ion acceleration region proportionally, and hence increases collisions such as charge exchange and ionization, which cause the secondary ions impinging on the suppressor grid. This is the reason why I_{dec} is approximately proportional to P_{fil}, though the beam divergence does not vary.

From the above results, we conclude that the beam divergence does scarcely depend on the gas pressures P_{vac} and P_{fil} in our operating range.

4.4.3 Relation between Field Intensity Ratio and Beam Divergence

According to the results of analytical estimation in the thin lens approximation[36] or two-dimensional computer simulation of ion beam trajectories,[37] the field intensity ratio f is an important parameter for the beam optics in the two-stage acceleration system. Here, the field intensity ratio f is defined by $f = V_{ext}d_{acc}/d_{ext}(V_{acc} + V_{dec})$, that is, the ratio of electric field intensity in the extraction gap to that in the acceleration gap. According to the numerical results in Subsection 4.3, the beam divergence is improved with the decrease of f. Here, we investigate the effect of f on the beam optics experimentally.

The beam divergences are measured as functions of gap distances d_{ext} and d_{acc} and total beam energy $V_{ext} + V_{acc}$ in the range of drain current I_{acc} = 0.1 - 1.6 A. Figure 4-16 shows the beam divergence as a function of perveance per hole in the case of d_{ext} = 6 mm, d_{acc} = 8 mm, and $V_{ext} + V_{acc}$ = 50 keV, where perveance per hole is defined by $I_{acc}(V_{ext} + V_{acc})^{-3/2}$ divided by the number of apertures. This result shows that the reduction of the ratio V_{ext}/V_{acc} makes the minimum beam divergence ω_{min} decrease for the fixed gap distances, while we must allow the reduction of optimum perveance P_{opt}. The latter is defined by the perveance that gives the minimum beam divergence when the extraction current I_{acc} is changed. It also shows that the divergence increases very gradually above the optimum perveance. Such tendency is not observed in the single-stage acceleration. This is

preferable to obtain a low divergent and high perveance beam. Furthermore, the influence of source plasma density fluctuation on the beam divergence can be reduced when the dependence of beam divergence on the perveance is weak. Figure 4-17 summarizes wide variety of data from the view point of the dependence of minimum beam divergence and optimum perveance on the field intensity ratio. From this figure, it is seen that the decrease of f makes ω_{min} and P_{opt} decrease, as is expected by the analytical and numerical estimation. However, too small field intensity ratio (smaller than 0.2) again increases the divergence. This may be that the strong lens effect overwhelm the space-charge expansion of the beam.

4.4.4 Effects of Aperture Shape on Beam Divergence

Effects of aperture shape on beam optics have previously been studied in some detail using ion sources with a single-stage, accel-decel structure.[38,39,40] Some aperture shape in the plasma electrode makes a beam with very low divergence (smaller than one degree). In the two-stage configuration, the aperture shape in the gradient grid also has great influence on beam optics. When the field intensity ratio is smaller than unity, the gradient grid acts as a positive lens. In such a case, the aberrations of the lens can be reduced by chamfering the aperture edge on the downstream side. Figure 4-18 shows the types of aperture shape studied. All the above experiments are made by using the type 1 grid.

Figure 4-19 shows the beam divergence as a function of perveance per hole for aperture types 1 - 4, where $d_{ext} = d_{acc} = 6$ mm, $V_{ext} = 15$ kV and $V_{acc} = 35$ kV. Chamfering of apertures in the gradient grid together with that in the plasma grid is indeed effective, and the beam divergence is reduced by about 0.5 degree in the type 4 grid, compared with the type 1 grid.

In Fig. 4-20, the dependences of the beam divergence on the perveance per hole in type 4 are compared with those in type 1, for a set of values of V_{ext} and V_{acc}, when $V_{ext} + V_{acc} = 50$ kV and $d_{ext} = d_{acc} = 6$ mm. Also shown in Fig.4-21 is the effectiveness of chamfering in the cases of $V_{ext} + V_{acc} = 60$ kV and 70 kV. Thus, considerable improvement of the beam divergence is made, which does scarcely depend on the field intensity ratio or total beam energy.

However, the improvement is somewhat retracted as the field intensity ratio becomes large. This is mainly due to the fact that the lens effect of the gradient grid is decreased as the ratio f becomes large, and the chamfering for the improvement of aberrations is no more meaningful.

To increase the beam current further, we chamfered the plasma grid deeper by the indication of Ref.(40) and (41). By using this grid, we have obtained a 70 kV, 2.0 A ion beam with beam divergence of 1.4 degree, where d_{ext} = 6 mm, d_{acc} = 4.5 mm, V_{ext} = 30 kV and V_{acc} = 40 kV.

4.4.5 Heat Loading of the Grids

The energy deposition to the extraction grids will be a critical problem for ion sources of the long beam duration. In the case of single-stage acceleration, the heat loading of the extraction grids is studied in some detail.[42] Here, the heat loading of the extraction grids (Grid Type 4) is measured in the case of two-stage acceleration.

In Fig.4-22, the beam divergence, the electric current flowing into each grid, and the calorimetrically measured heat loading of each grid and beam dumper are shown as a function of extraction current I_{acc}, where $d_{ext} = d_{acc} = 6$ mm, $V_{ext} = 15$ kV, $V_{acc} = 35$ kV, $P_{fil} = 0.07$ Torr and $P_{vac} = 1.6 \times 10^{-4}$ Torr. The heat loading is normalized by the beam power, $I_{acc} \times V_{tot}$. The decel current I_{dec} depends on the number of energetic ions and neutrals impinging on the suppressor grid. Such particles consist of extracted primary ions and the secondary particles produced by the charge exchange or ionization, together with backstreaming ions from the beam plasma. Therefore, I_{dec} depends on the beam divergence, extracted current I_{acc} and the pressure in the ion acceleration region. In most cases studied here, I_{dec} is smaller than $0.1 \times I_{acc}$. The current of gradient grid I_g is negatively small at lower extraction current I_{acc}. At higher I_{acc}, however, a sharp increase of I_g is observed. The positive I_g indicates that the direct interception by the gradient grid is dominant, while the negative I_g indicates that the secondary electron inflow due to the interception by the suppressor grid is dominant. Therefore, the

sharp increase of I_g at higher I_{acc} suggests that the meniscus of ion emitter becomes convex. The plasma grid receives the most loading, 1.7 kW or about 200 Watts per cm^2 at I_{acc} = 1.2 A, where the loading by arc discharge is included. This value is about a factor of 2 greater than we have already demonstrated for 10 sec operation.[15] The heat loading of suppressor grid is the smallest of the four grids. It should be noted that the divergence and the ratios of heat loading of various grids are minimized when I_g is nearly equal to zero.

In the case of V_{ext} = 10 kV, V_{acc} = 40 kV, where the field intensity ratio is very small (0.25) compared to the above case (See Fig.4-23), the characteristics are similar to those of Fig.4-22 for $I_g < 0$. For $I_g > 0$, however, the heat loading of the gradient and the plasma grid increases appreciably compared with that of the exit or the suppressor grid, in spite of the decrease of beam divergence. Large heat loading of the gradient and the plasma grid is due to an increase of impinging ions on the suppressor and the gradient grid. However, the ions passing through the gradient grid are focused by the strong positive lens effect, which makes the divergence very small. It is noticeable that, although the heat loading of the plasma and the gradient grid is very large, the beam with very low divergence smaller than one degree can be obtained at $I_{acc} \simeq 0.6$ A beyond which it was impossible to extract ion beams.

In order to decrease the impinging ions on the gradient grid which cause the large heat loading of the plasma and

the gradient grid, we tried to enlarge the aperture diameter of the gradient grid to 4.3 mm. By this method, we can reduce the heat loading of the gradient and the plasma grid by about 50 % without changing the beam optics for the worse at $I_{acc} \simeq 0.6$ A. Although the heat loading again increases with I_{acc} for $I_{acc} > 0.6$ A, we can raise the maximum extractable current to 0.8 A. This is also due to the decrease of impinging ions on the gradient grid, which makes it possible to operate the ion source stably.

4.4.6 Conclusion

The beam divergence does scarcely depend on the operating gas pressure both in the ion source (P_{fil}) and in the beam flight region (P_{vac}), when P_{fil} = 0.05 - 0.15 Torr and $P_{vac} = 2 \times 10^{-4} - 2 \times 10^{-3}$ Torr. We find the tendency that the minimum beam divergence is improved with the decrease of field intensity ratio f, while one must allow the decrease of optimum perveance, the perveance at which the beam divergence is minimum. However, too small f (smaller than 0.2) again increases the divergence. For obtaining a high perveance and low divergent beam, it is preferable that f takes the value about 0.3 - 0.5. The chamfering of apertures in the gradient grid is effective together with that of the plasma grid, to improve the beam divergence. By chamfering the plasma grid deeper, we can extract a beam of 2.0 A at 70 keV from the 5 cm diam grid with 83 apertures. The ratio of heat loading of each grid decreases with the improvement of beam optics, and their level is typically less than about 2 % at the optimum perveance. For the case of small f (smaller than 0.25), however, only the heat loadings of the plasma and the gradient grid become very large in spite of the decrease of beam divergence, above a certain perveance value. These large loadings can be reduced by enlarging the aperture diameter in the gradient grid.

§5. Focusing by Beamlet Steering in Two-Stage Acceleration System

5.1 Introduction

The beam line length of the injector becomes up to several to ten meters with the increase of target plasma thickness. The long beam line diminishes the effectiveness of beamlet steering, and imposes the further improvement of beamlet optics. In the initial design of JT-60 injector where 4 ion sources with 12 cm diam. extraction grid are applied, the improvement of injection power by beamlet steering is several percent. However, we can expect the improvement above 10 %, in the present design where 2 ion sources with larger extraction grid (12 cm × 27 cm rectangular grid) are used. Then, we can see that the focusing of indivisual beamlet to the injection port is necessary to improve the injector efficiency, as discussed in Section 2. Here, the beamlet steering by aperture displacement in the two-stage acceleration system (Model A) is investigated by introducing a thin lens model.

5.2 Derivation of Steering Characteristic

Two methods can be considered for the beamlet steering; one is by aperture displacement, and the other is by curved electrodes. In the latter case, extraction grids should be spherically concave so that the curvature center of the grids corresponds to the focal point. For instance, the 24 cm diam. grid shall be concave only by 0.90 mm compared with plain disk grid at the axis, if we need the focal point 8 m apart from the grid.

On the other hand, the focusing by aperture displacement has been investigated both in experiments and in a simple model in thin lens approximation.[16] Here, we applied this simple model to the beamlet steering in the two-stage acceleration system.[37,43,44] An aperture with a different potential gradient on each side acts as a lens with focal length $Z_f = 4V/(E_2 - E_1)$ for a round aperture and $Z_f = 2V/(E_1 - E_2)$ for a slit aperture, respectively. Here, E_1 and E_2 are, respectively, the electric field on each side of the extraction grid, and eV is the energy of the beam which pass through the grid, where e is the ionic charge. The two-stage acceleration system consists of two lenses. The first lens is formed by the electric fields in the first and the second gaps, and the second lens is formed by the electric fields in the second and the third gaps. The electric field in the third gap, however, is almost negligible compared with the others. According to the results of the computer simulation, $E_1 = k_1 V_1/d_1$ with $k_1 = 0.9 \sim 1.0$ and $E_2 = k_2(V_2 + V_3)/d_2$ with $k_2 = \sim 1.0$ in the wide range of the

beam current density, if the gap distances are enough larger than the aperture radius.[37,45] Here, V_1, V_2+V_3, and V_3 are the potential drop in the first, the second, and the third gaps, respectively. d_1 and d_2 are the distances of the first gap and the second gap, respectively. Therefore, we choose $E_1 = V_1/d_1$ and $E_2 = (V_2+V_3)/d_2$, though in the single-stage acceleration the deflection angle by aperture displacement agrees well with the experimental results when we put $E_1 = 4V_1/3d_1$ in the plane parallel approximation.[16] The focal length of the first and the second lenses are given as follows; for a round aperture;

$$F_1 = 4V_1/(E_2 - E_1) = 4d_2pg(g - p)$$
$$F_2 = 4(V_1 + V_2)/(E_3 - E_2) = -4d_2(1 + p) \qquad (5\text{-}1)$$

and for a slit aperture;

$$F_1 = 2V_1/(E_2 - E_1) = 2d_2pg(g - p)$$
$$F_2 = 2(V_1 + V_2)/(E_3 - E_2) = -2d_2(1 + p) \quad , \qquad (5\text{-}2)$$

where p is the potential ratio defined by $p = V_1/(V_2+V_3)$ and g is the gap ratio defined by $g = d_1/d_2$. There are three cases in the aperture displacement, which are the displacement in the plasma grid(a), the gradient grid(b), and the suppressor grid(c), respectively (See Fig.5-1). Case (c) is equivalent to the simultaneous aperture displacement in the plasma and gradient grid. It is natural that

the displacement of the exit grid does scarcely cause the deflection of beamlet axes because of the small difference of electric field intensity on the both side of the grid as well as the large beam energy corresponding to the final beam energy. The ratios of reflection angle of the beamlet θ to the radial displacement of the grid Δ are given as follows for each case,

$$\text{(a)}\quad \frac{\theta}{\Delta_1} = \left(\frac{1}{F_2} - \frac{1}{d_2 - F_1} \right) \cdot \frac{F_1 - d_2}{F_1} = \frac{5g - 5p - 4p^2}{16 d_2 p (1+p) g} \tag{5-3}$$

for a round aperture

$$\text{(b)}\quad \frac{\theta}{\Delta_2} = \left(\frac{1}{F_2} - \frac{1}{d_2} \right) \cdot \frac{d_2}{F_1} = \frac{(4p+5)(g-p)}{16 d_2 p (1+p) g} \tag{5-4}$$

for a round aperture

$$\text{(c)}\quad \frac{\theta}{\Delta_3} = \frac{1}{F_2} = \begin{cases} -\dfrac{1}{4d_2(1+p)} & \text{for a round aperture} \\ -\dfrac{1}{2d_2(1+p)} & \text{for a slit aperture} . \end{cases} \tag{5-5}$$

Figure 5-2 shows the deflection characteristics for each case as a function of field intensity ratio f, which is defined by the ratio of electric field intensity in the extraction gap to that in the acceleration gap, and is equal to p/g. According to the results in experiments using a duopigatron ion source with two-stage acceleration system[46] or two-dimensional computer simulation of ion beam trajectories,[16] the field intensity ratio f is an important parameter

for the beam optics in the two-stage acceleration system. Namely, the beam optics does scarcely depend on the aspect ratio, gap ratio g, and potential ratio p, so long as f is fixed. The smaller beam divergence can be obtained as the ratio f becomes smaller. However, higher perveance can be obtained with the increase of f. To obtain high perveance and low divergent beam, the value of f around 0.5 is adequate. From the results in Fig.5-2, the first two cases are inadequate in that the displacement characteristic depends largely on the parameter f. In the third case, however, the deflection does scarcely depend on f. In other words, the focal length does not vary in the wide range of operating condition of an ion source.

5.3 Discussion

The good displacement must be larger than the mechanical inaccuracy ±~0.1 mm, but far smaller than the aperture diameter to keep good beam optics;

$$\text{Mechanical inaccuracy } \pm 0.1 \text{ mm} \ll \Delta \ll \text{Aperture Diameter.} \tag{5-6}$$

Now, when f = 0.5, $d_1 = d_2 = 6$ mm, focal length $Z_f = 8$ m, and the radius of the extraction grid is 12 cm, the displacement Δ_3 at the periphery of the grid is about 0.5 mm for a round aperture. This is the practical value of the dispacement. Consequently, the beamlet steering by aperture displacement is possible for the case of two-stage configuration.

The analysis here by the thin lens approximation has some limitations, because the above results include no dependence on the radius of the apertures or the thickness of the electrodes. In general, the error in the above analysis increases appreciably when the radius of the apertures becomes comparable or smaller than the thickness of the electrode or becomes larger than the gap distances between the electrodes. However, the error may be small because we use the electric field intensity E_1, E_2 and E_3 obtained in the two-dimensional computer simulation.

§6. Conclusion

As one of the works in research and development of high power ion source for JT-60 neutral beam injector, the beam optics in two-stage acceleration system has been investigated both numerically and experimentally. The results obtained contribute to the design of JT-60 neutral beam injector.

The beam line length of the injector becomes up to several to ten meters with the increase of target plasma thickness. The long beam line diminishes the effectiveness of beamlet steering, and imposes the further improvement of beamlet optics. In the initial design of JT-60 injector where 4 ion sources with 12 cm diam. extraction grid are applied, the improvement of injection power by beamlet steering is several percent. However, we can expect the improvement above 10 %, in the present design where 2 ion sources with larger extraction grid (12 × 27 cm rectangular grid) are used. The accurate orientation of the total beam to the center of the injection port proved to be very important for the injector with small acceptance. The beam deflection above 0.5 degree is sure to decrease the injection efficiency appreciably.

A computer simulation code for cylindrically symmetric ion beams has been developed for the design of ion extraction/acceleration system and the optimum operating condition of an ion source. The validity of this code is checked by comparing the experimental data with the computational results. It is seen that the computer code simulates the actual ion beam trajectories fairly well.

By making use of this code, two-stage ion beam optics was investigated. It is found that the beam optics in the two-stage acceleration system depends strongly on the field intensity ratio f. Namely, the beam optics scarcely depends on the gap ratio, and potential ratio, so long as the field intensity ratio is fixed. The smaller beam divergence can be obtained as the ratio f becomes smaller. However, higher perveance can be obtained with the increase of f. To obtain high perveance and low divergent beam, the value of f around 0.5 is adequate. It is pointed out that the optimum operation conditions (grid potentials and gap distances) can be determined uniquely once the ratio f and the total beam energy are given.

These computational results agree well with the experimental data obtained by using a duopigatron ion source with two-stage acceleration system. It is found experimentally that the gradient grid current is deeply related to the beam optics and the grid heat loading.

Finally, the beamlet steering by aperture displacement was investigated in the two-stage acceleration system by introducing a thin lens approximation. It is found that the simultaneous aperture displacement in the plasma and gradient grids (or suppressor and exit grids) is adequate in that the steering characteristic does scarcely depend on the field intensity ratio which determines the two-stage ion beam optics.

From the above results, we are fully convinced of obtaining a proton beam which satisfy the requirements imposed on the JT-60 neutral beam injector.

Acknowledgement

Foremost the author expresses his sincere gratitude to Professor T.Uchida of University of Tokyo, whose continuing encouragements and advice have been invaluable. He also acknowledges Associate Professor N.Inoue who first introduced him to the field of neutral beam injection for fusion devices.

The author expresses his sincere gratitude to Drs. H.Shirakata, Y.Obata, and S.Mori for their continuing support and encouragement in the development of an ion source with two-stage accelerator. Participation of many members of the plasma heating laboratory is gratefully acknowledged. In particular, Dr. S.Matsuda provided many valuable insight and suggestions to this work. He wishes to thank T.Ohga, S.Tanaka and Y.Okumura for their valuable discussions and assistance in the experiments. Thanks are also due to T.Fujie and S.Ogawa for their assistance in making the program of ion beam simulation code.

This research was performed at the Japan Atomic Energy Reseach Institute as one of the works in the development of high power ion source for JT-60 neutral beam injector.

References

1. H.P. Furth : Nucl. Fusion 15 (1975) 487
2. D.L. Jassby : Nucl. Fusion 17 (1977) 309
3. A. Gibson et al. : in Toroidal Plasma Confinement (Proc. 3rd Int. Symp., Garching, Fed. Rep. Germany, 1973) B16-1
4. J.G. Cordey, et al. : Nucl. Fusion 15 (1975) 441
5. K. Bol, et al. : Phys. Rev. Lett. 32 (1974) 661
6. L.A. Berry, et al. : in Plasma Physics and Controlled Nuclear Fusion Research (Proc. 5th Int. Conf., Tokyo, 1974) 1, IAEA, Vienna (1975) 113
7. J.W.M. Paul, et al. : in Plasma Physics and Controlled Nuclear Fusion Research (Proc. 6th Int. Conf., Berchtesgaden, 1976) 2, paper IAEA-CN-35/A17, IAEA, Vienna
8. TFR Group : in Plasma Physics and Controlled Nuclear Fusion Research (Proc. 6th Int. Conf. Berchtesgaden, 1976) 1, IAEA, Vienna (1977) 69
9. V.S. Vlasenkov, et al. : in Plasma Physics and Controlled Nuclear Fusion Research (Proc. 6th Int. Conf., Berchtesgaden, 1976) 1, IAEA, Vienna (1977) 85
10. T. Sugawara, et al. : Japan Atomic Energy Research Institute Report JAERI-M 7043 (1977)
11. D.L. Jassby : Nucl. Fusion 17 (1977) 373
12. S. Matsuda, et al. : Japan Atomic Energy Research Institute Report JAERI-M 7655 (1978).
13. S. Matsuda : Japan. J. Appl. Phys. 13 (1974) 1630.

14. Y. Ohara, S. Matsuda, H. Shirakata and S. Tanaka : Japan Atomic Energy Research Institute Report, JAERI-M 6438 (1976) [in Japanese]

15. S. Matsuda, et al. : Proc. 2nd Large Tokamak Meeting, Princeton, 1976 (IAEA, Vienna, 1976)

16. L.D. Stewart, J. Kim and S. Matsuda : Rev. Sci. Instrum. 46 (1975) 1193

17. Y. Ohara : Japan Atomic Energy Research Institute Report JAERI-M 6757 (1976) [in Japanese]

18. P.T. Kirstein, G.S. Kino, and W.E. Waters : Space-Charge Flow (McGraw-Hill, New York, 1967)

19. A. Septier ; Focusing of Charged Particles (Academic Press, New York, 1967)

20. D.G. Bate : Culham Laboratory Report CLM-R53 (1966)

21. J.L. Harrison : J. Appl. Phys., 39 (1968) 3827

22. W.S. Cooper, K. Halbach, and S.B. Magyary : Proc. 2nd Symp. on Ion Sources and Formation of Ion Beams, California, 1974 (Lawrence Berkeley Lab., Berkeley, 1975) Paper II-1

23. E.F. Jaeger and J.C. Whitson : Oak Ridge National Laboratory Report ORNL-TM-4990 (1975)

24. S.A. Self : Phys. of Fluids 6 (1963) 1762

25. R.C. Davis, O.B. Morgan, L.D. Stewart and W.L. Stirling : Rev. Sci. Instrum. 43 (1972) 278

26. T. Shibata, T. Itoh, H. Shirakata and T. Sugawara : Japan Atomic Energy Research Institute Report JAERI-M 6990 (1977) [in Japanese]

27. R.C. Davis, T.C. Jernigan, O.B. Morgan, L.D. Stewart, W.L. Stirling : Oak Ridge National Laboratory Report, ORNL-TM-4657, (1974).

28. W.R. Baker, K.H. Berkner, W.S. Cooper, K.W. Ehlers, W.B. Kunkel, R.V. Phle, and J.W. Stearns : Plasma Physics and Controlled Nuclear Fusion Research (Proc. 5-th Int. Conf. Tokyo, 1974) IAEA-CN-33/D2-2

29. D.A. Aldcroft, J.N. Burcham, H.C. Cole, M. Cowlin, R.S. Hemsworth, J. Sheffield, E. Speth : Culham Laboratory Report, CLM-P414, (1975)

30. M. Fumelli, F.P.G. Valckx : Report of the Association EURATOM, EUR-CEA-FC-809, (1976).

31. J.R. Coupland, T.S. Green, D.P. Hammond, and A.C. Riviere : Rev. Sci. Instrum, 44, (1973) 1258

32. L.D. Stewart, et al. : 1st Topical Meeting on the Tech. of Controlled Nuclear Fusion, San Diego (1974)

33. T. Sugawara and Y. Ohara : Japan. J. appl. Phys. 14, (1975) 1029

34. Y. Ohara and T. Sugawara : Japan Atomic Energy Research Institute Report, JAERI-M 5929 (1974)

35. T. Ohga, et al. : Japan Atomic Energy Research Institute. Report JAERI-M 7604 (1978)

36. E. Thompson : Proc. 2nd Symp. on Ion Sources and Formation of Ion Beams, California, 1974 (Lawrence Berkaley Lab., Berkeley, 1975) Paper II-7

37. Y. Ohara : Japan Atomic Energy Research Institute Report, JAERI-M 6813 (1976)

38. W.S. Cooper, K.H. Berkner and R.V. Pyle : Nucl. Fusion 12 (1972) 263

39. E. Thompson : Proc. 2nd Symp. on Ion Sources and Formation of Ion Beams, California, 1974 (Lawrence Berkeley Lab., Berkeley, 1975) Paper II-3

40. L.R. Grisham, C.C. Tsai, J.H. Whealton and W.L. Stirling : Rev. Sci. Instrum., 48 (1977) 1037

41. J.R. Coupland, T.S. Green, D.P. Hammond and A.C. Riviere : Rev. Sci. Instrum., 44 (1973) 1258

42. L.D. Stewart, R.C. Davis, T.C. Jernigan, O.B. Morgan, D.E. Schechter, and W.L. Stirling : Proc. 2nd Symp. on Ion Sources and Formation of Ion Beams, California, 1974 (Lawrence Berkeley Lab., Berkeley, 1975) Paper II-8

43. J.H. Whealton : Rev. Sci. Instrum. 48 (1977) 1428

44. Y.Ohara : Japan. J. Appl. Phys. 18 (1979) 351.

45. J. Kim, J.H.Whealton and G. Schilling : J. Appl. Phys. 49 (1978) 517.

46. Y.Ohara, Y. Arakawa, H. Horiike, U. Kondoh, S. Matsuda, T. Ohga, Y. Okumura and H. Shirakata : Proc. 7th Symp. on Engineering Problems of Fusion Research, Knoxville (1977) 273.

Figure Captions

Fig.2-1 Schematic illustration of the extraction grid and the injection port. The point (X_p, Y_p, Z_p) indicates the center of beamlet emitted from the point (X_g, Y_g, O).

Fig.2-2 Dependence of the beam fraction passing through the injection port F on the beam line length Z_p, as a parameter of beamlet divergence. The broken curves indicate the case without beam focusing.

Fig.2-3 Relation between the beam fraction F and the beamlet divergence ω, when R_g = 6 cm, R_p = 20 cm and $Z_p = Z_f$ = 8 m.

Fig.2-4 Dependence of the beam fraction F on the beamline length Z_p, as a parameter of grid radius R_g, where R_p and ω are fixed to 20 cm and 1.0°, respectively. The solid line indicates the case with beam focusing.

Fig.2-5 Relation between the beam deflection angle θ and the beam fraction F, as a parameter of beamlet divergence ω. The radial displacement of the beam at $Z = Z_p$ is denoted by Δ.

Fig.3-1 Block diagram of computer program.

Fig.3-2 Showing the relationship between the points A, B, C, D and O used in Eq.3-4.

Fig.3-3 Schematics of the duopigatron ion source with single hole extraction electrodes. The beam divergence is measured by the Faraday Cup placed 44 cm apart from the extraction electrode.

Fig.3-4 Schematics of the ion extraction region. The computed beam divergences are compared with the experimental data for this configuration.

Fig.3-5 Comparison of the measured beam divergence with calculated one.

Fig.4-1 Two models of the two-stage acceleration system (Model A and Model B).

Fig.4-2 Illustration of lens actions in the two-stage acceleration system.

Fig.4-3 Dependence of the minimum beamlet divergence of the 75 keV proton beam on the shape of aperture in the first grid.

Fig.4-4 Dependence of the minimum beamlet divergence of the 75 keV proton beam on the aspect ratio a in the case of single stage acceleration. The accel gap distance is fixed to be 23.7 mm.

Fig.4-5 Dependence of the minimum divergence on the field intensity ratio f for the fixed acceleration voltage of 75 kV (a), and the dependence of the total extracted current from the 12 cm diam. grids with 40 % transparency on f (b), where the gap distances are scaled such that either d_1 or d_2 may coincide with the breakdown limit, while the other still satisfys the relation $d > (V/50)^2$.

Fig.4-6 Dependence of ω_{min} and P_{opt} (or I_{tot}) on the field intensity ratio for the proton beam accelerated at V = 75 kV from the 3.5 mm diam. aperture, where gap distance d_1 and d_2 are chosen to be the breakdown limit.

Fig.4-7 Beam trajectories calculated by the computer code IONORB for typical values of f ; (a) f = 1.2, J = 600 mA/cm^2, $\omega = 1.04^\circ$, (b) f = 0.8, J = 500 mA/cm^2, $\omega = 0.83^\circ$, (c) f = 0.5, J = 400 mA/cm^2, $\omega = 0.77^\circ$, (d) f = 0.4, J = 350 mA/cm^2, $\omega = 0.72^\circ$, (e) f = 0.3, J = 300 mA/cm^2, $\omega = 0.74^\circ$.

Fig.4-8 Dependences of ω_{min} and P_{opt} (or I_{tot}) on f, when the gap distances are determined by the equation $d = (V/40)^2$(kV, cm) instead of $d = (V/50)^2$.

Fig.4-9 Relation between the divergence and the aperture diameter, where the total current is fixed to be 15 A.

Fig.4-10 Changes of the beamlet divergence and the total extraction current (triangular points), when the gap distance is increased from the reference points denoted by the circular points at f = 0.5, 0.8 and 1.2.

Fig.4-11 Typical examples of beam trajectories in the three-stage acceleration system ; (a) $f_1 = 0.5$, $f_2 = 0.5$, J = 550 mA/cm^2, $\omega = 0.58^\circ$ and (b) $f_1 = 0.37$, $f_2 = 1.0$, J = 400 mA/cm^2, $\omega = 0.63^\circ$.

Fig.4-12 Duopigatron ion source with two-stage acceleration system.

Fig.4-13 Schematics of the two-stage acceleration system Composed of four grids, and the power supply system.

Fig.4-14 Dependence of beam divergence and decel current I_{dec} on the pressure in the beam flight region P_{vac}.

Fig.4-15 Relation between the pressure in the ion source P_{fil} and the beam divergence. Decel current I_{dec} and required arc current I_{arc} are also plotted.

Fig.4-16 Beam divergence as a function of perveance per hole, where total beam energy is fixed to 50 keV.

Fig.4-17 Dependence of minimum beam divergence ω_{min} and optimum perveance P_{opt} on the field intensity ratio.

Fig.4-18 Types of aperture shapes studied.

Fig.4-19 Improvement of beam divergence by chamfering the aperture edges.

Fig.4-20 Dependences of beam divergence on perveance per hole in type 4 grid are compared with those in type 1, as parameters of V_{ext} and V_{acc}.

Fig.4-21 Dependences of beam divergence on perveance per hole in type 4 grid are compared with those in type 1, where total beam energy is 60 keV and 70 keV.

Fig.4-22 Divergence and grid current (upper) and calorimetrically measured heat loading of various grids and beam dumper (lower), vs. extraction current I_{acc}, where field intensity ratio is 0.43.

Fig.4-23 Divergence and grid current (upper) and calorimetrically measured heat loading of various grids and beam dumper (lower), vs. extraction current I_{acc}, where field intensity ratio is 0.25.

Fig.5-1 Three cases in the aperture displacement, which are the displacements in the plasma grid (a),

the gradient grid (b), and the suppressor grid (c), respectively.

Fig.5-2 Deflection angle divided by the aperture displacement θ/Δ for each case as a function of field intensity ratio f.

Table I Potential drops and gap distances when f is equal to 0.6 and 0.8.

f	V_1 (kV)	V_2 (kV)	d_1 (mm)	d_2 (mm)	ω_{min}
0.6	48.1	26.9	9.3	3.3	0.74°
0.8	42.8	32.2	7.3	4.7	0.80°

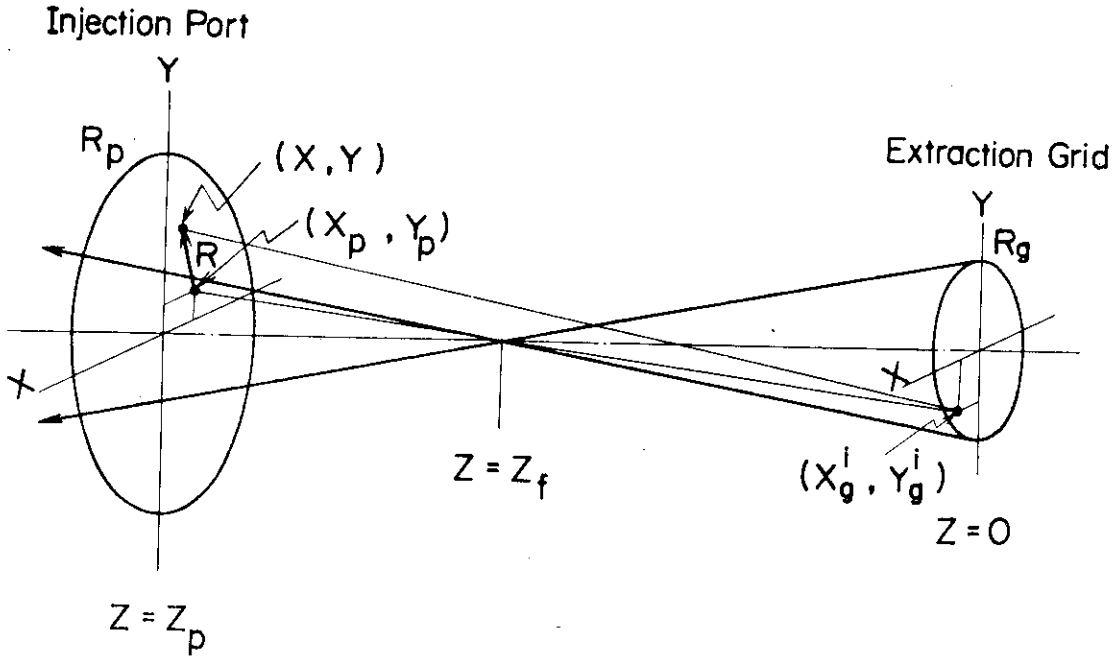

Figure 2-1

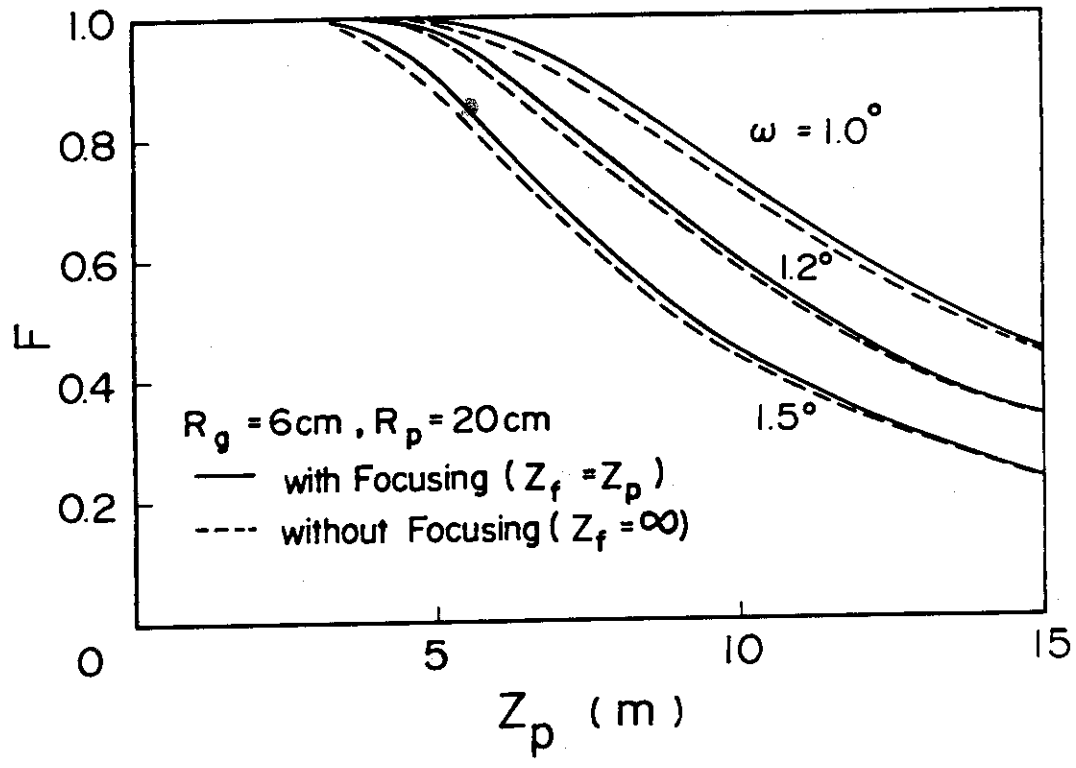

Figure 2-2

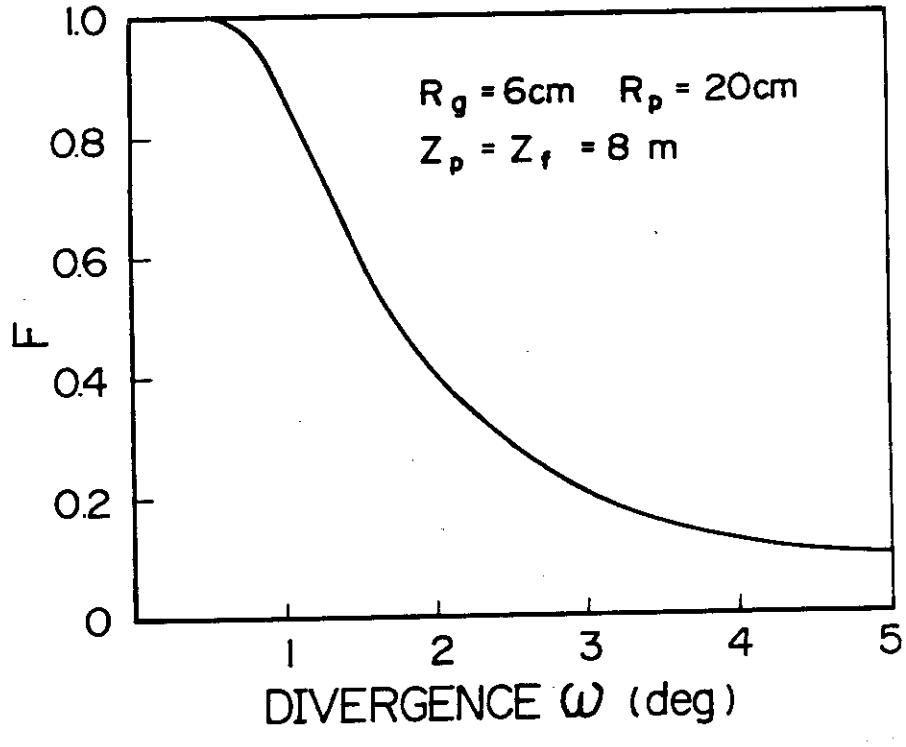

Figure 2-3

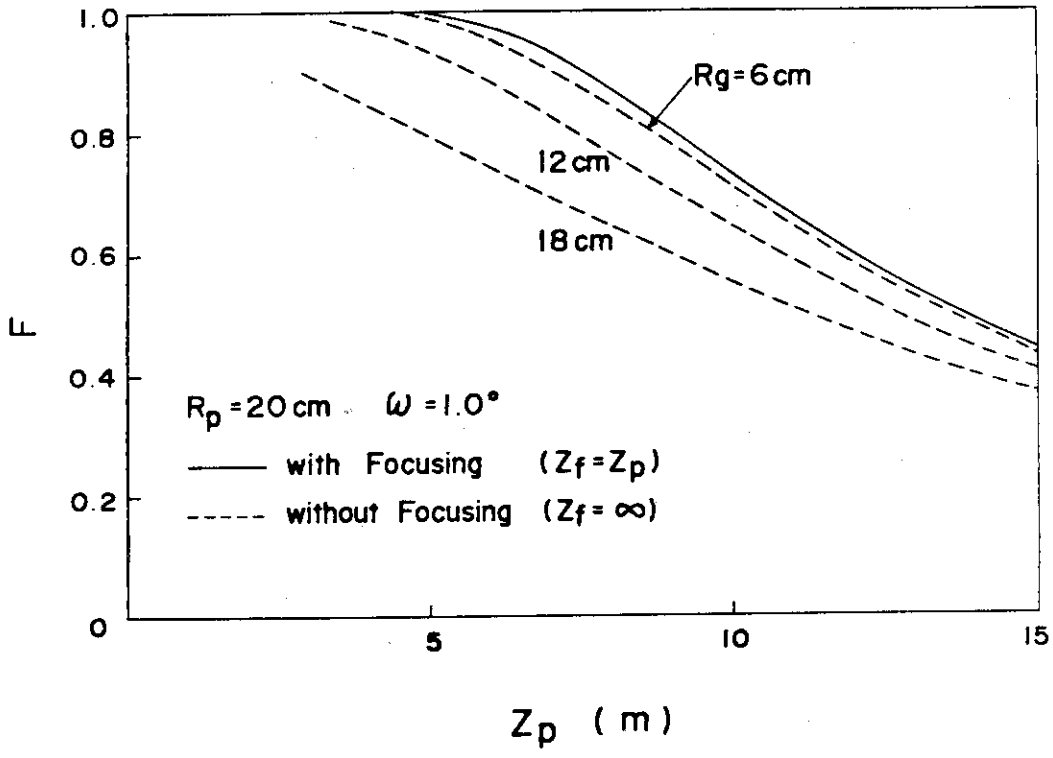

Figure 2-4

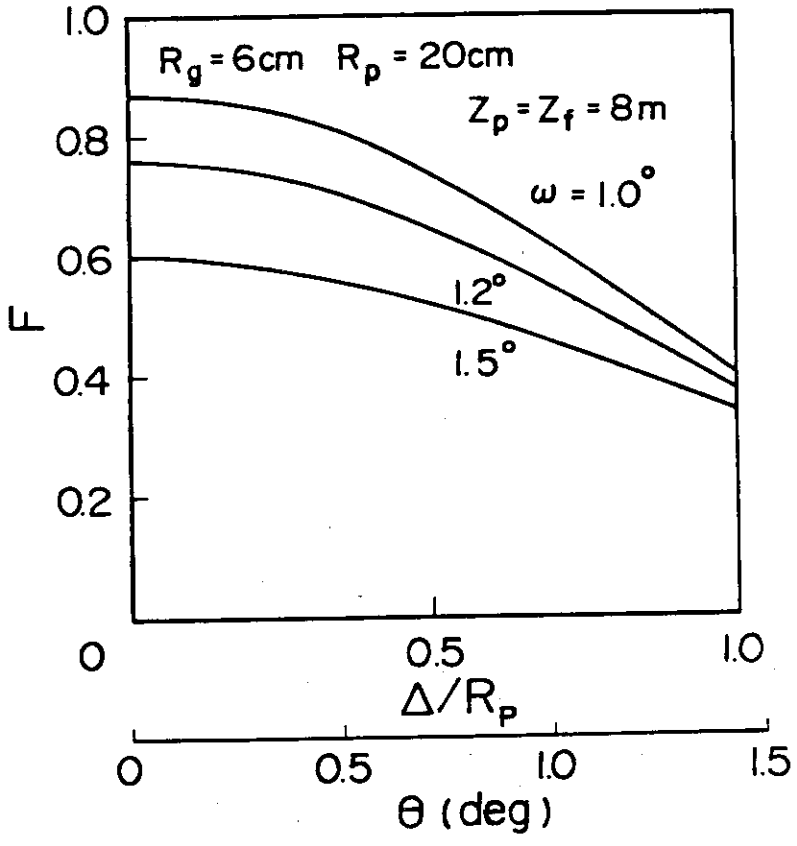

Figure 2-5

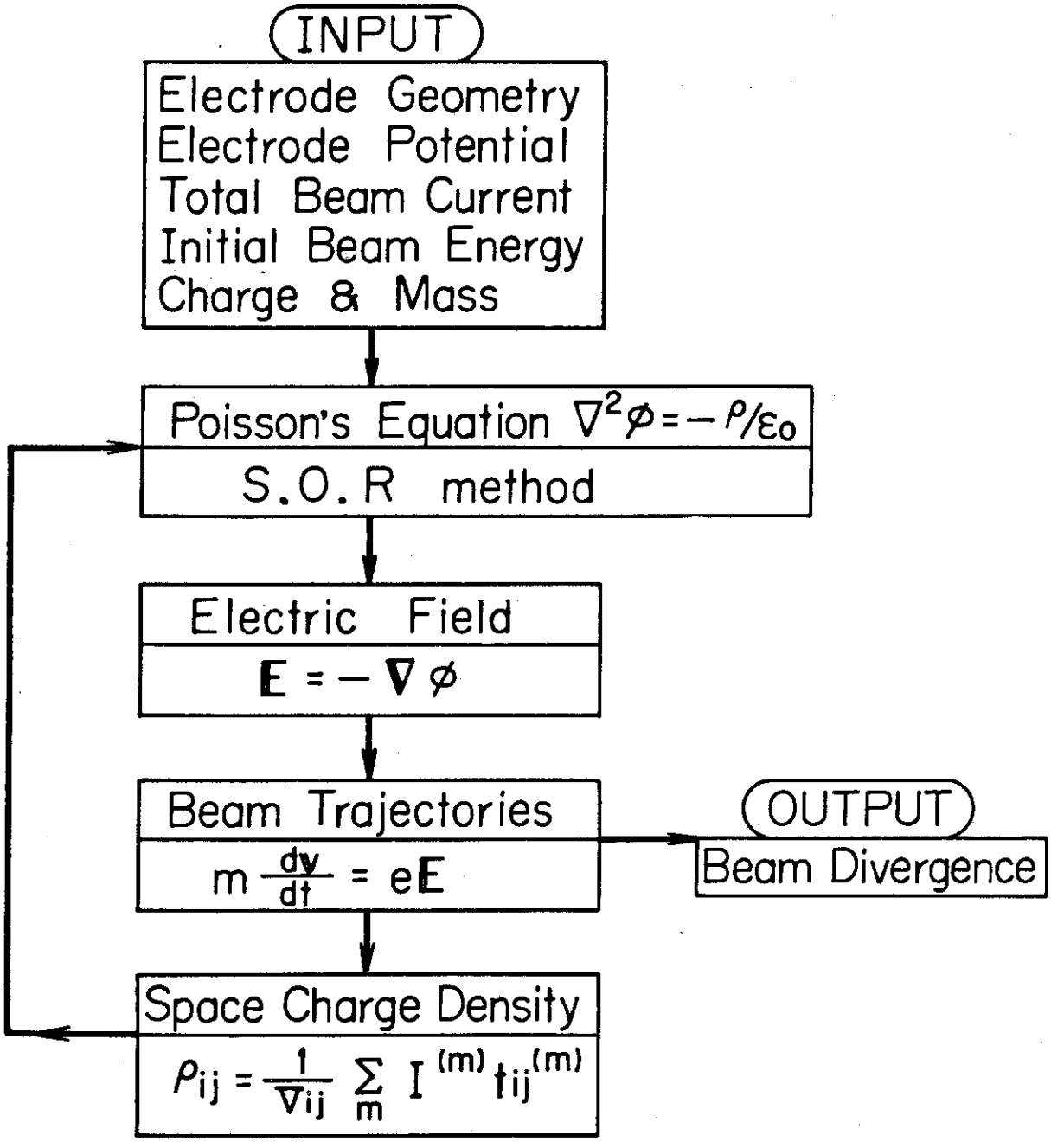
INPUT
Electrode Geometry
Electrode Potential
Total Beam Current
Initial Beam Energy
Charge & Mass
Poisson's Equation $\nabla^2\phi = -\rho/\varepsilon_0$
S.O.R method
Electric Field
$\mathbf{E} = -\nabla\phi$
Beam Trajectories
$m\frac{dv}{dt} = e\mathbf{E}$
OUTPUT
Beam Divergence
Space Charge Density
$\rho_{ij} = \frac{1}{\nabla_{ij}} \sum_m I^{(m)} t_{ij}^{(m)}$

Figure 3-1

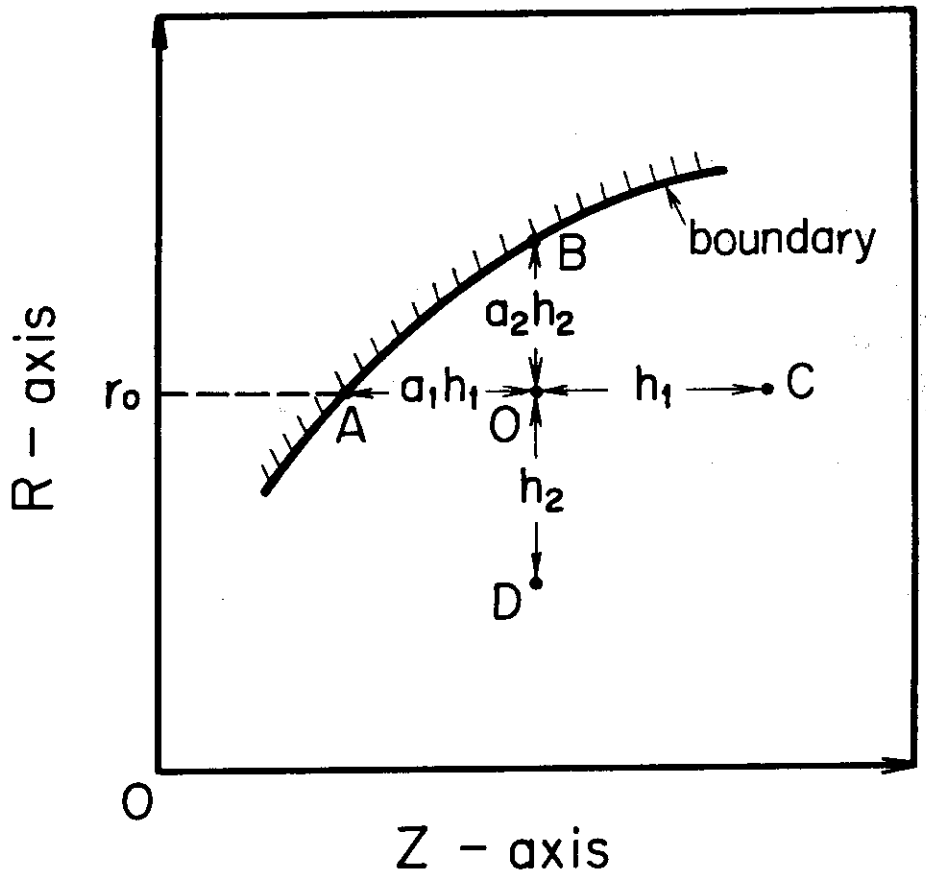

Figure 3-2

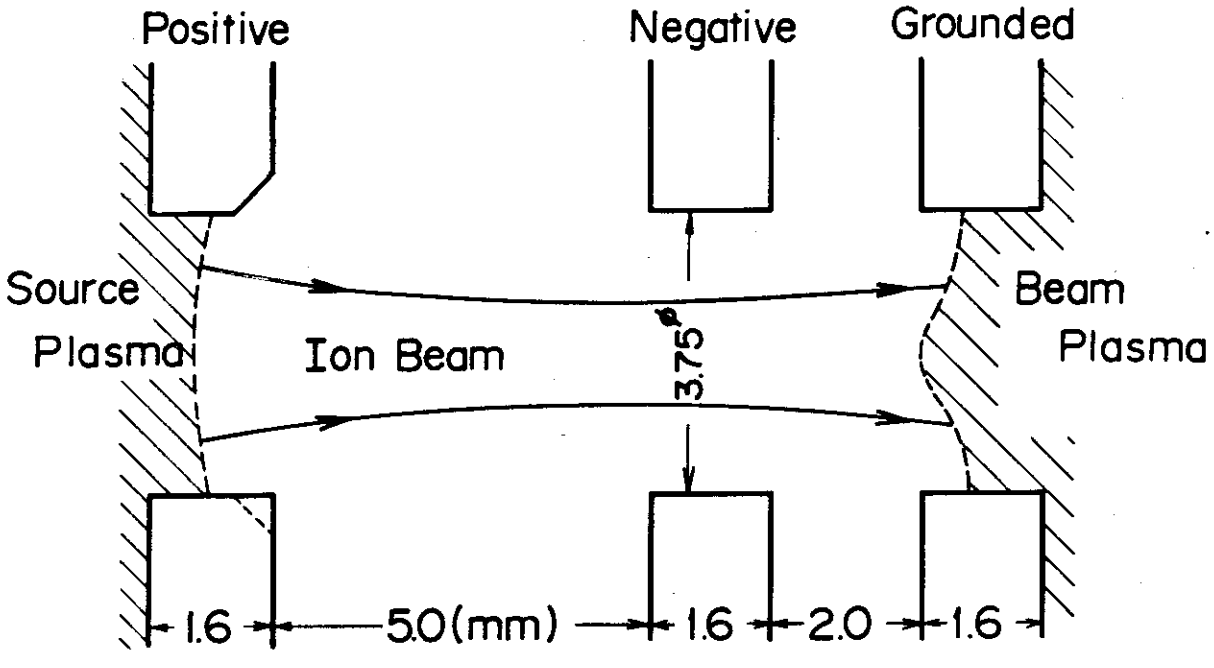

Figure 3-3

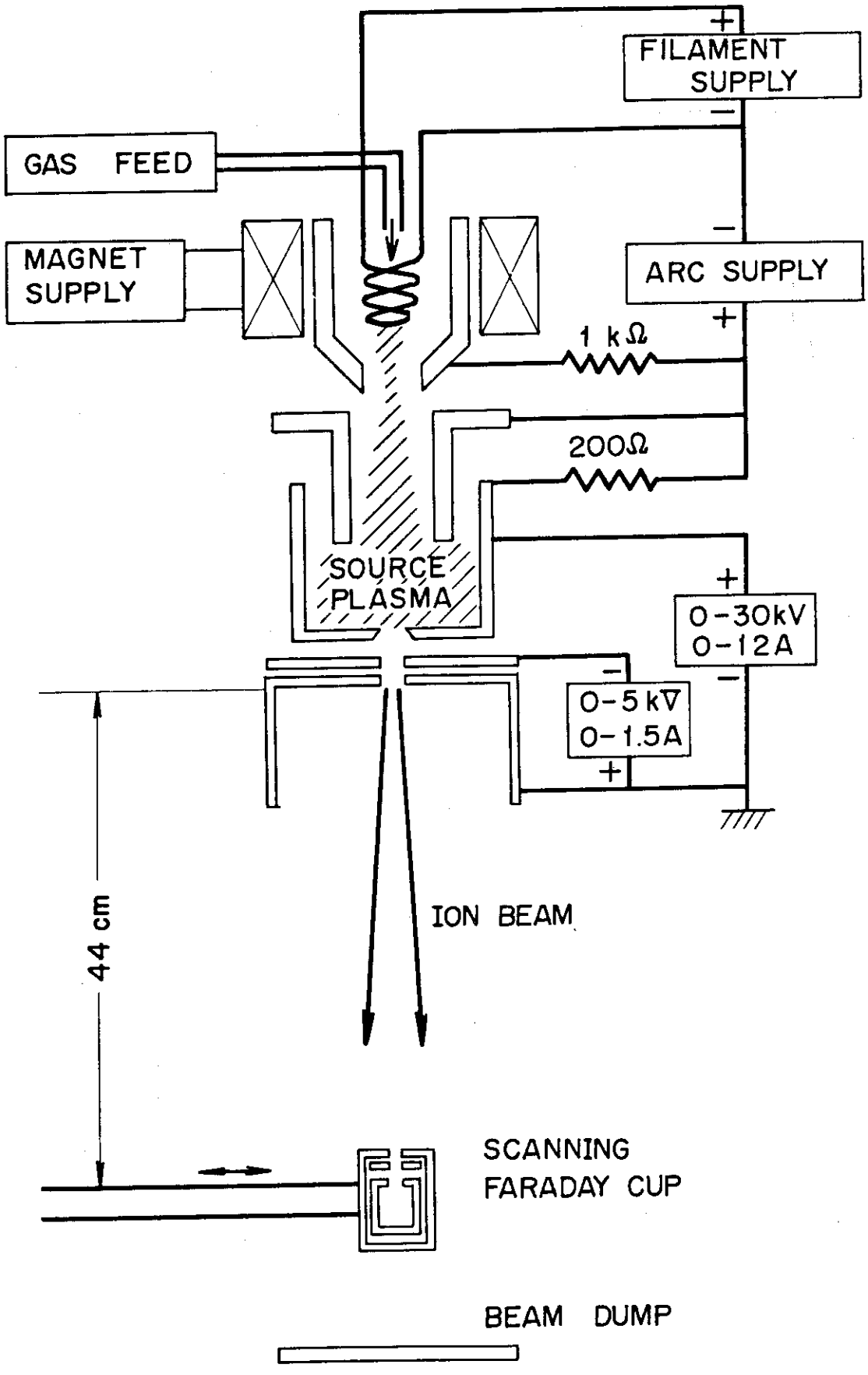
FILAMENT
SUPPLY
GAS FEED
MAGNET
SUPPLY
ARC SUPPLY
1 kΩ
200Ω
SOURCE
PLASMA
0-30kV
0-12A
0-5 kV
0-1.5A
44 cm
ION BEAM
SCANNING
FARADAY CUP
BEAM DUMP

Figure 3-4

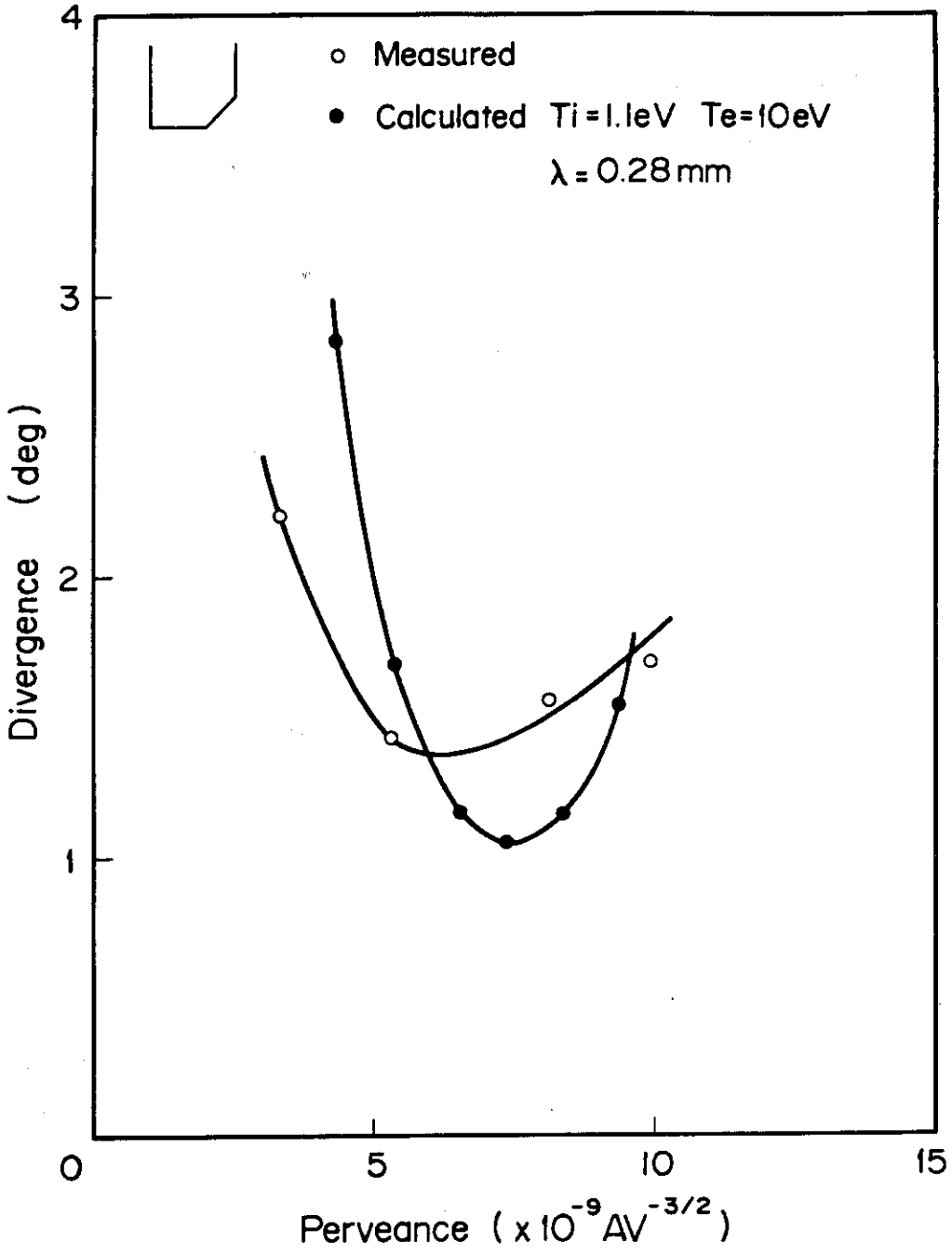
Measured
Calculated Ti=1.1eV Te=10eV
λ=0.28mm
Divergence (deg)
Perveance (x 10^-9 AV^-3/2)
0
1
2
3
4
5
10
15

Figure 3-5

Model A

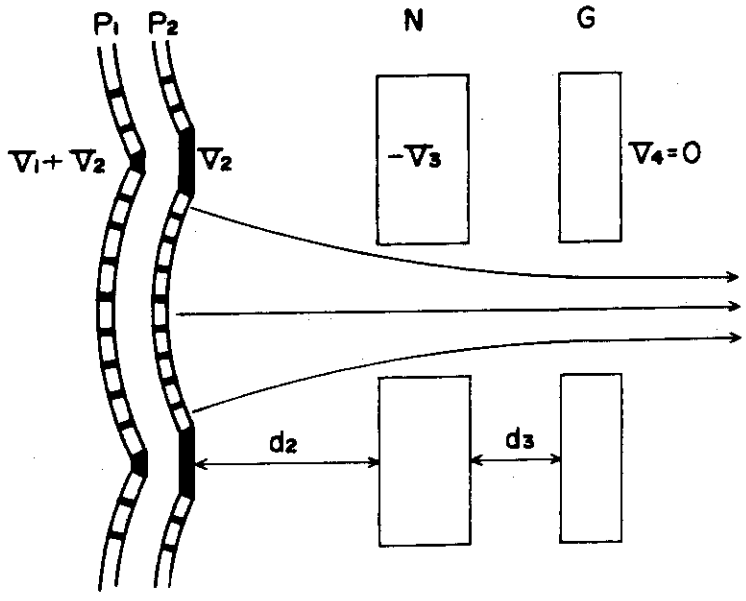

Model B

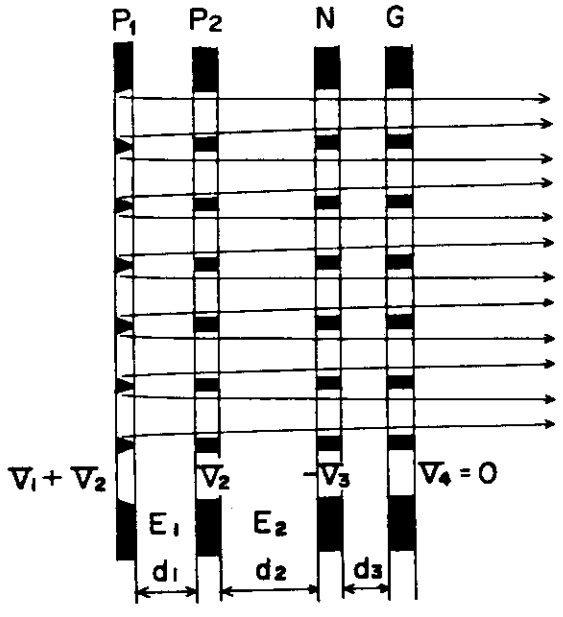

Figure 4-1

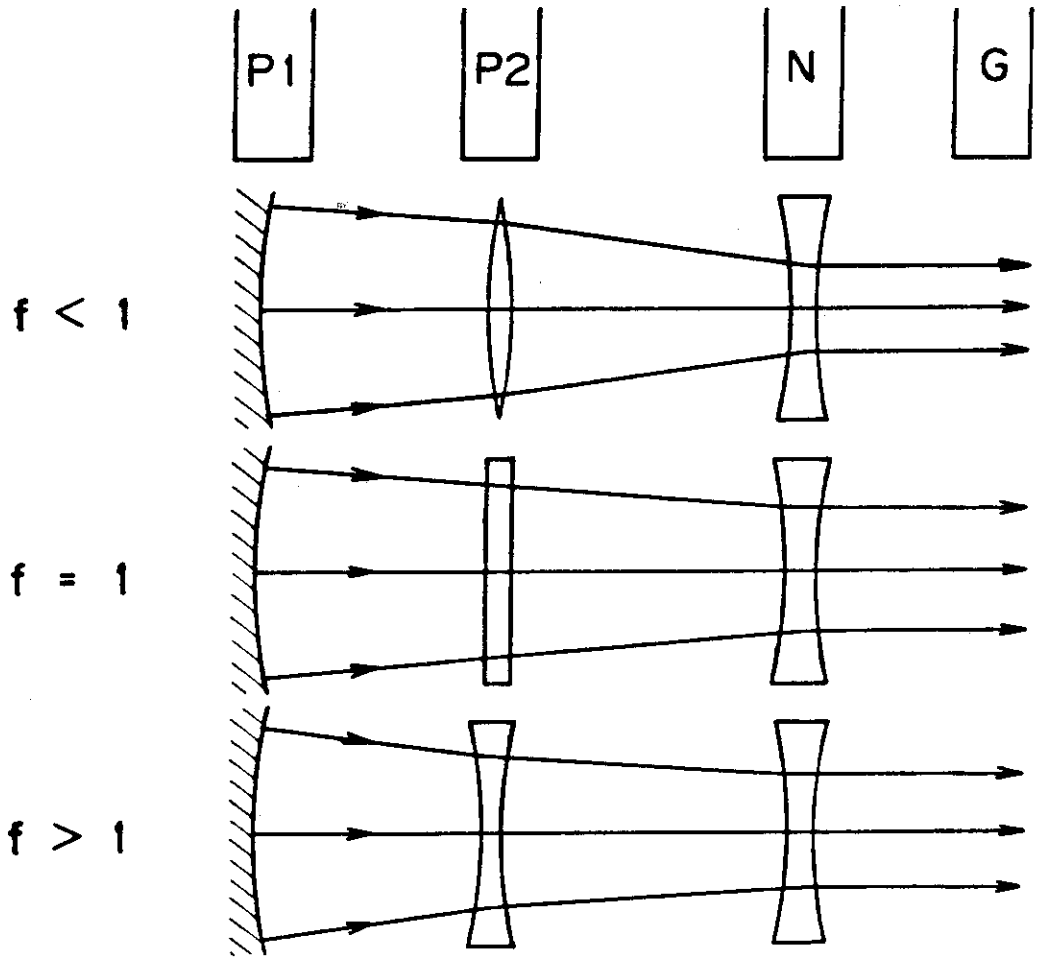

Figure 4-2

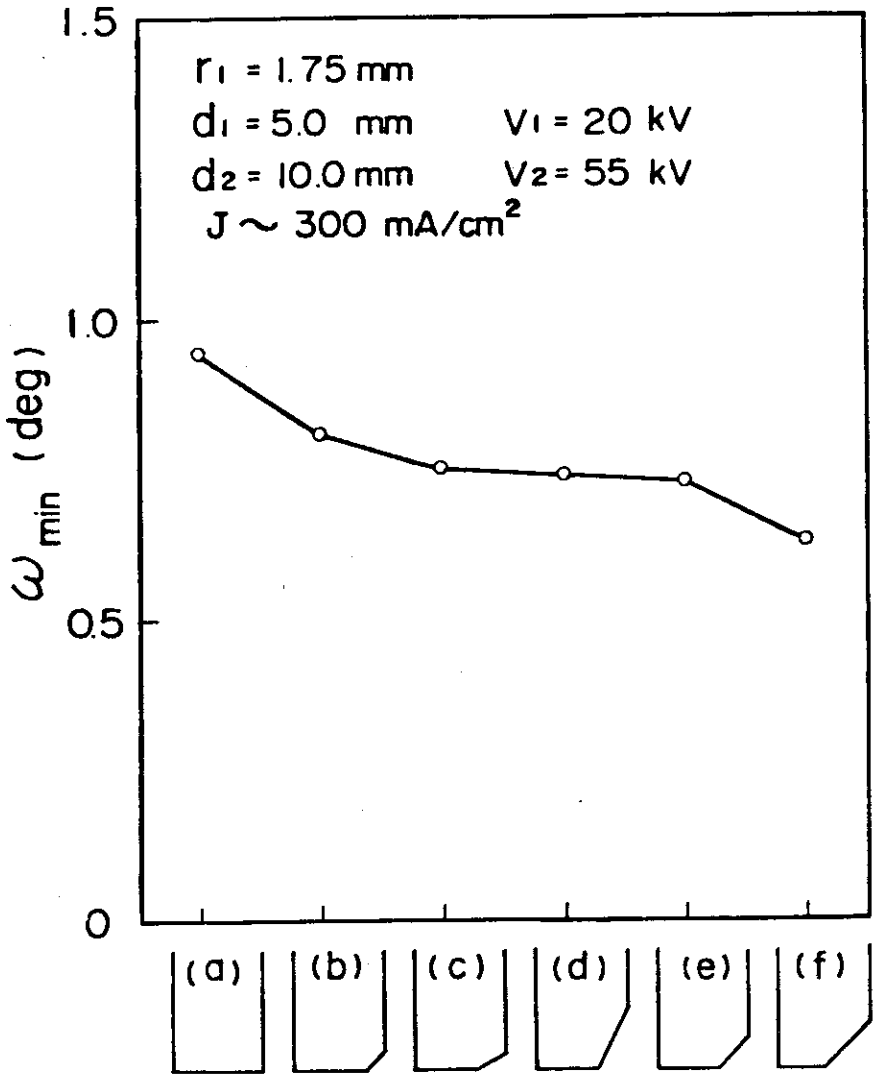

SHAPE OF APERTURE IN THE FIRST GRID

Figure 4-3

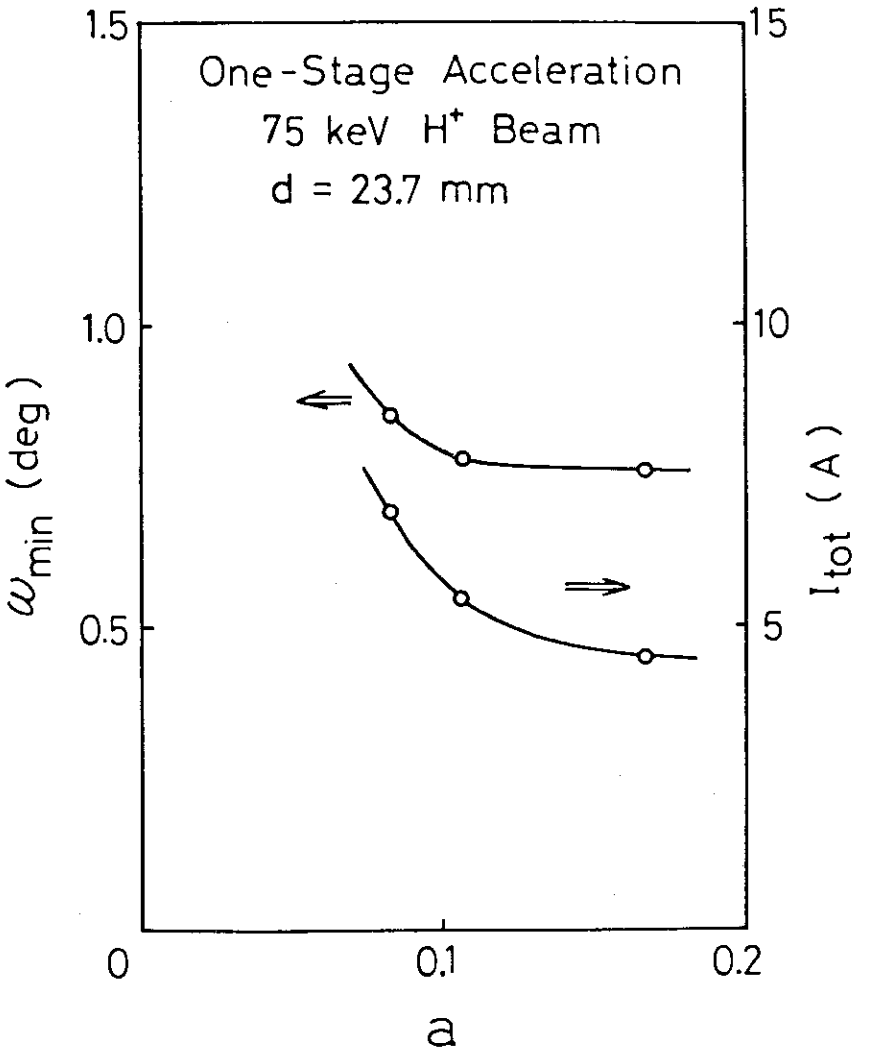

Figure 4-4

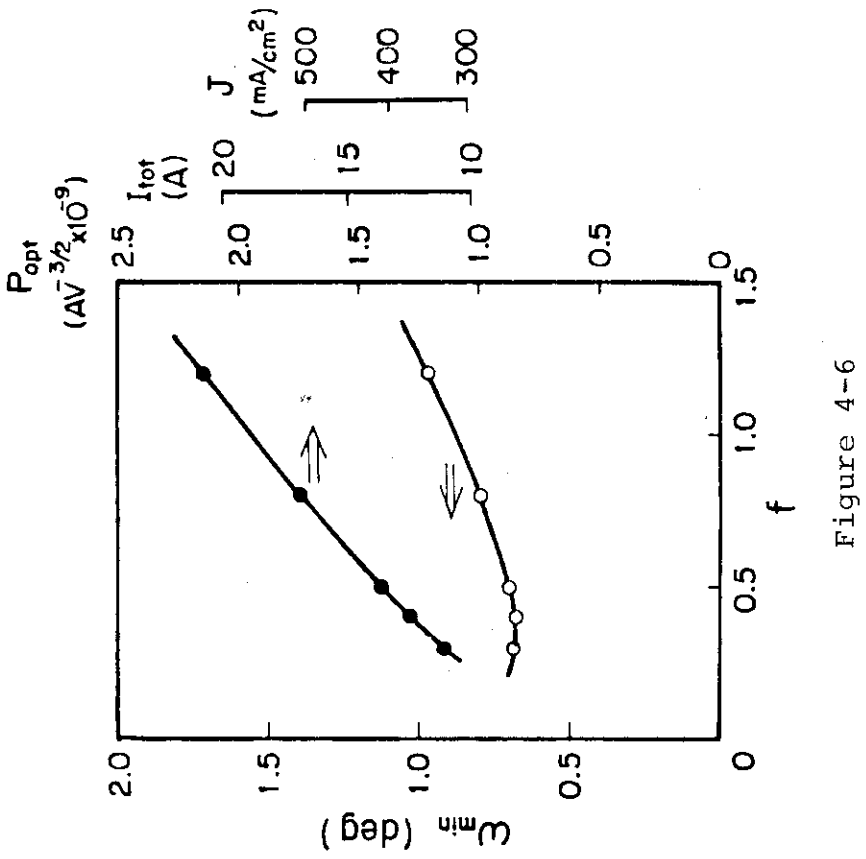

Figure 4-6

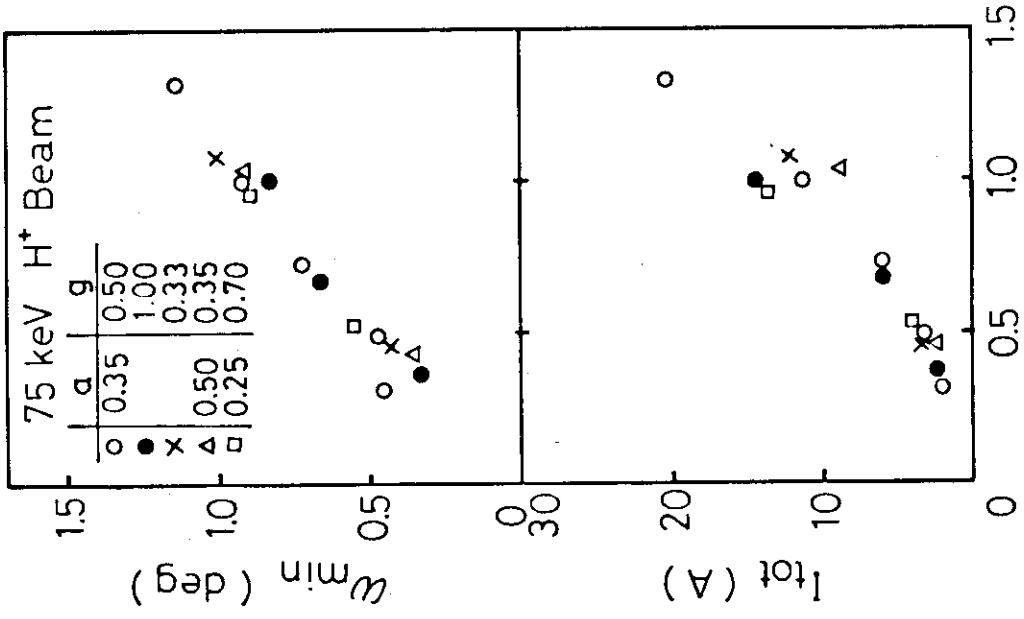

Figure 4-5

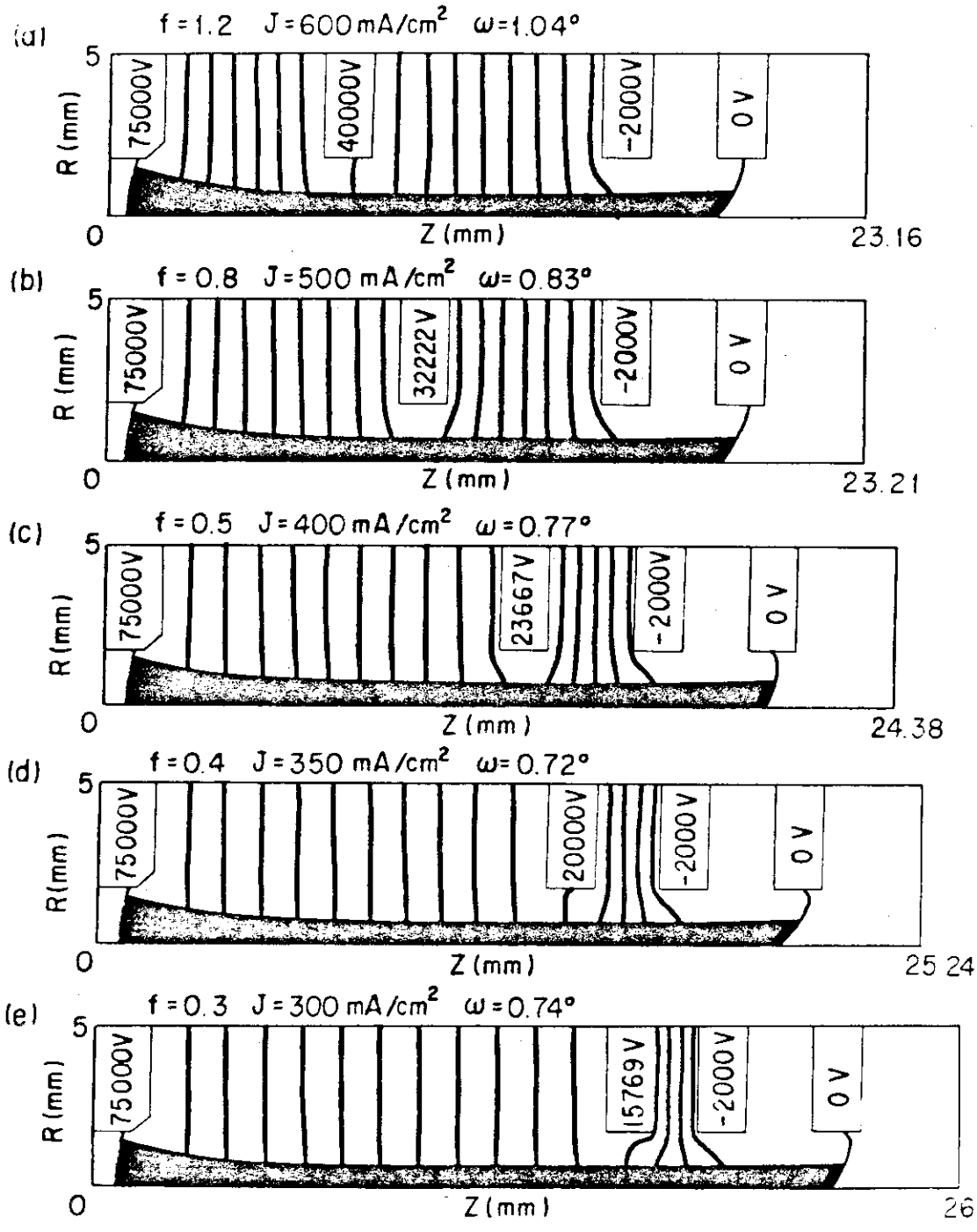
(a)
f = 1.2 J = 600 mA/cm² ω = 1.04°
75000V
40000V
-2000V
0 V
R (mm)
5
0
Z (mm)
23.16
(b)
f = 0.8 J = 500 mA/cm² ω = 0.83°
75000V
32222 V
-2000V
0 V
R (mm)
5
0
Z (mm)
23.21
(c)
f = 0.5 J = 400 mA/cm² ω = 0.77°
75000V
23667V
-2000V
0 V
R (mm)
5
0
Z (mm)
24.38
(d)
f = 0.4 J = 350 mA/cm² ω = 0.72°
75000V
20000V
-2000V
0 V
R (mm)
5
0
Z (mm)
25 24
(e)
f = 0.3 J = 300 mA/cm² ω = 0.74°
75000V
15769 V
-2000V
0 V
R (mm)
5
0
Z (mm)
26

Figure 4-7

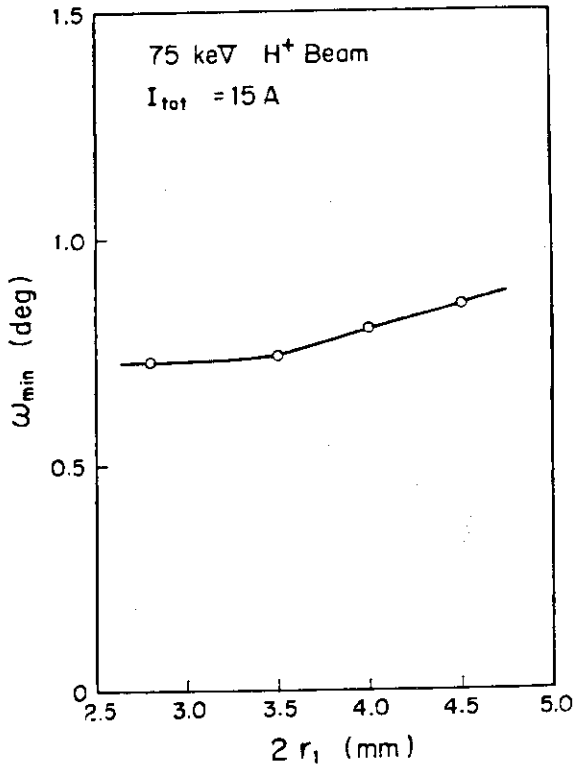

Figure 4-9

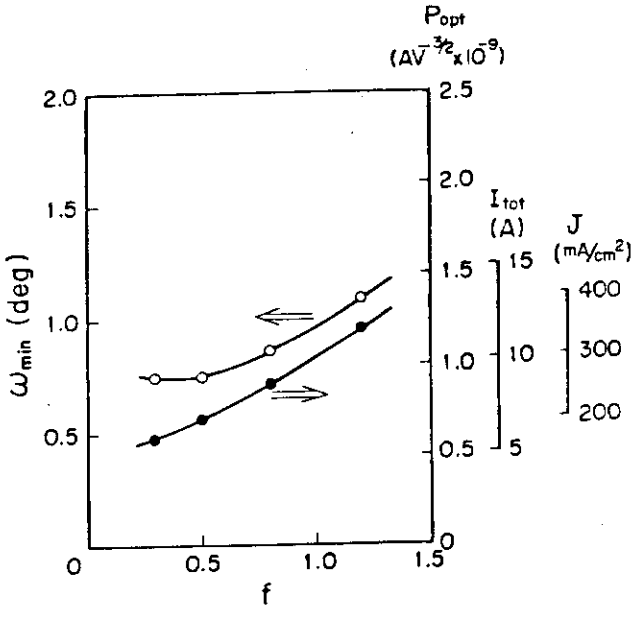

Figure 4-8

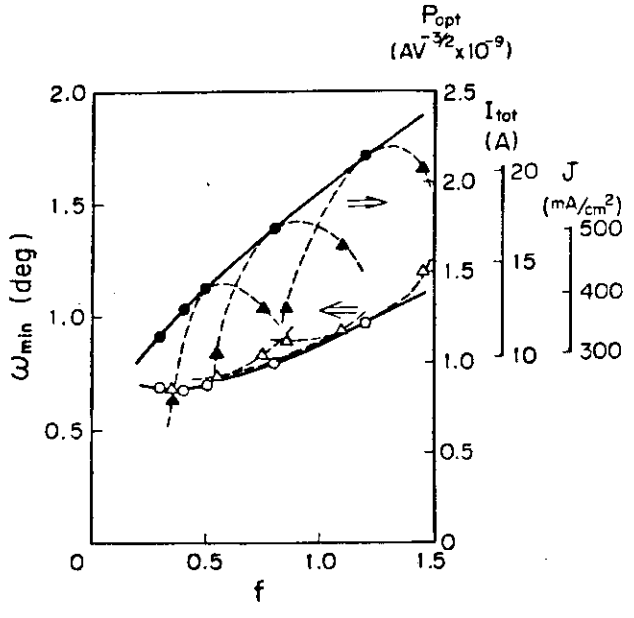

Figure 4-10

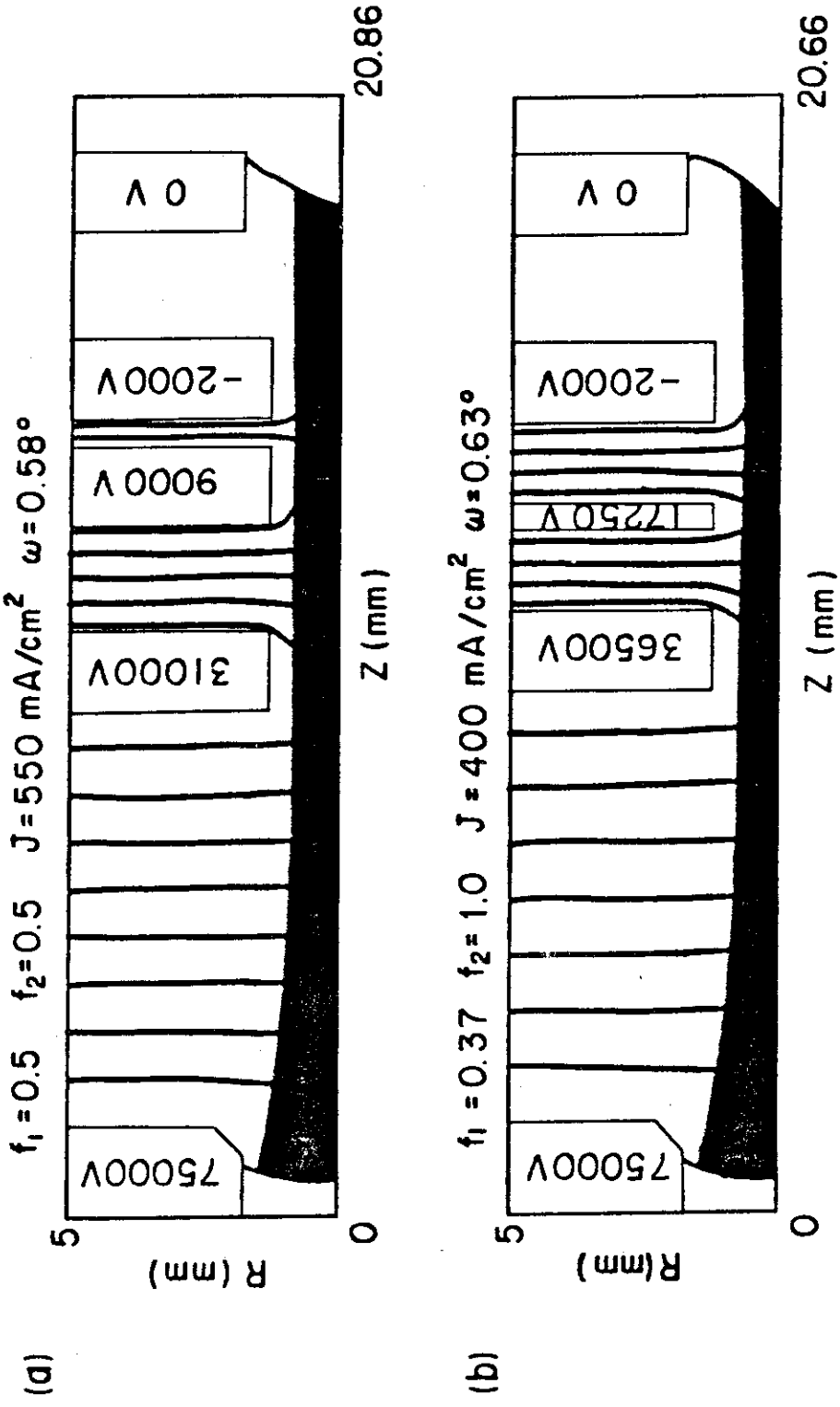
(a)
f_1=0.5 f_2=0.5 J=550 mA/cm^2 ω=0.58°
75000V
31000V
9000V
-2000V
0 V
R (mm)
5
0
Z (mm)
20.86
(b)
f_1=0.37 f_2=1.0 J=400 mA/cm^2 ω=0.63°
75000V
36500V
17250V
-2000V
0 V
R(mm)
5
0
Z (mm)
20.66

Figure 4-11

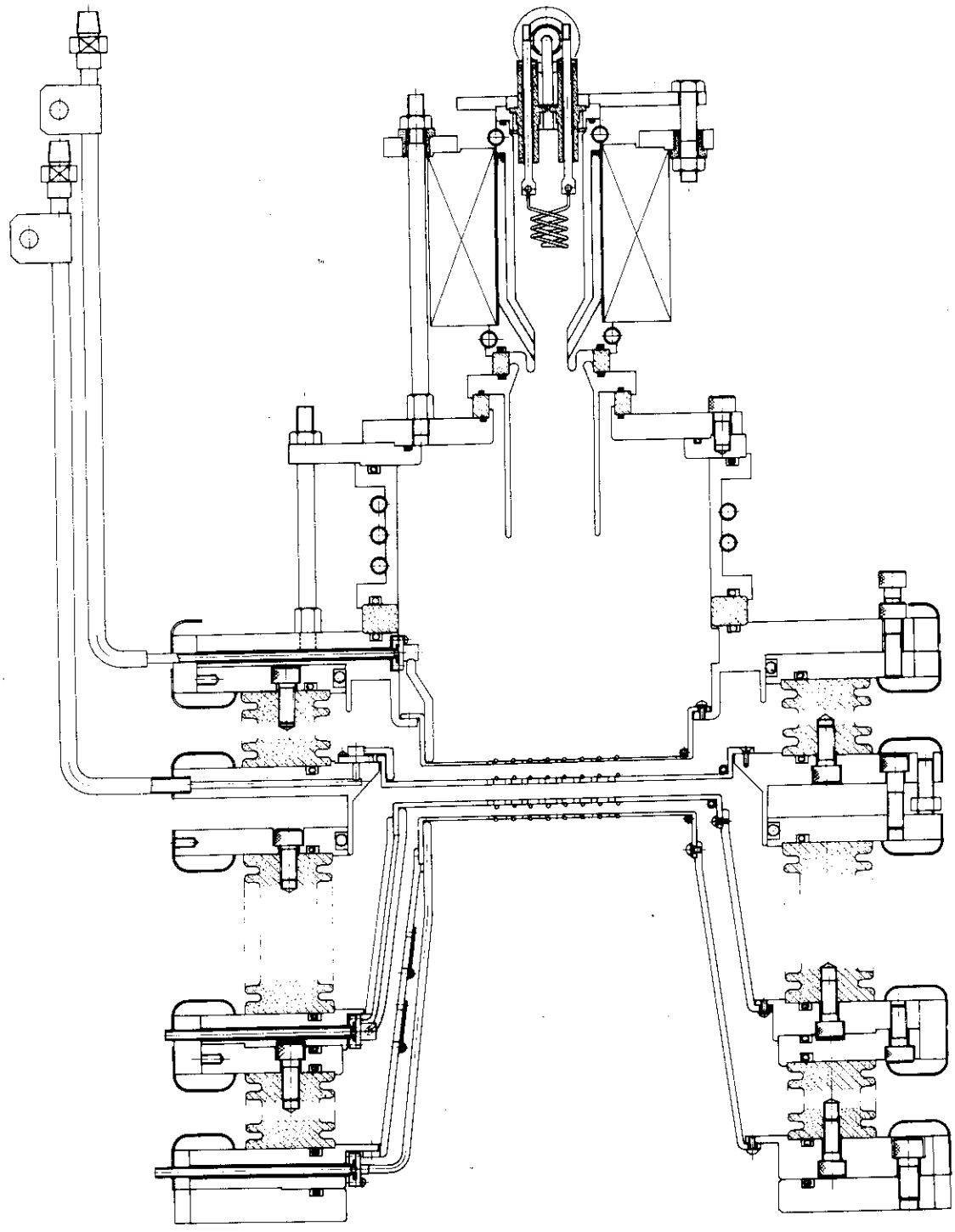

Figure 4-12

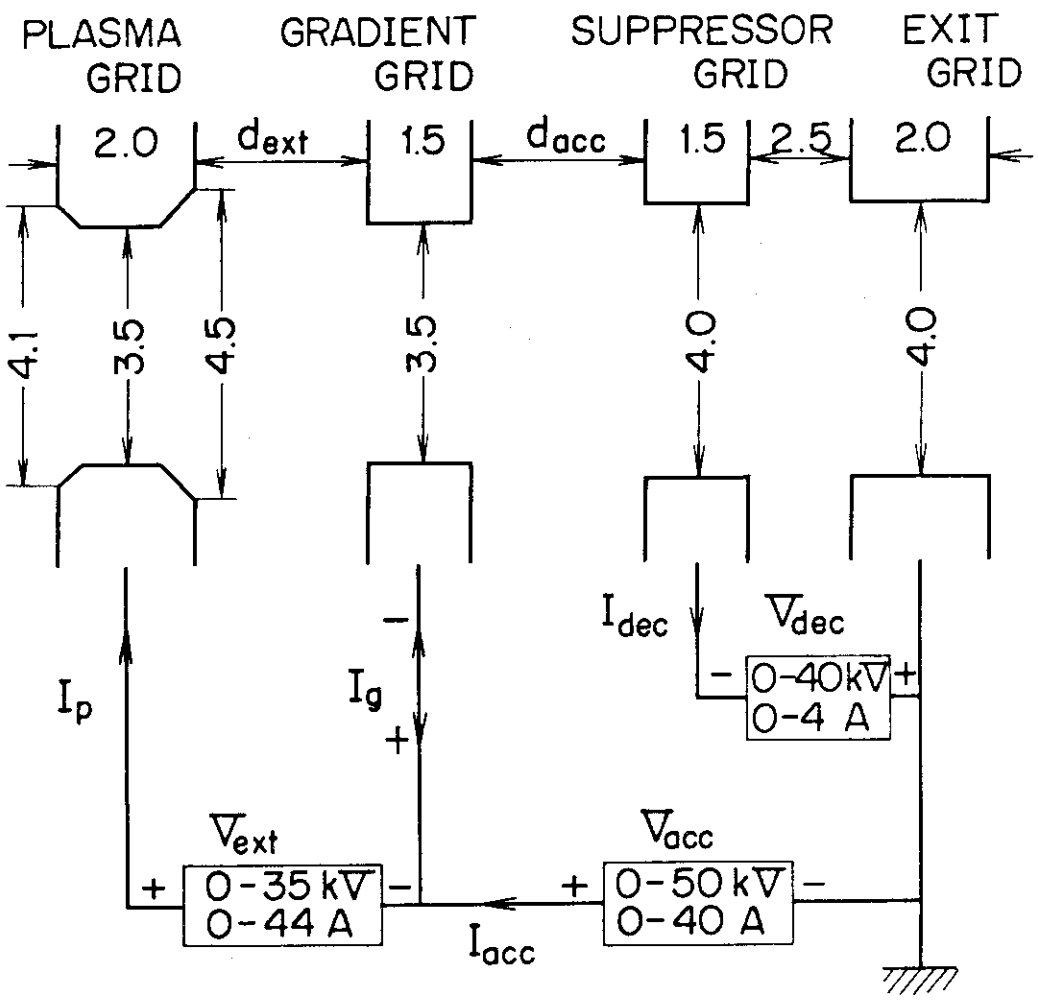
PLASMA GRID
GRADIENT GRID
SUPPRESSOR GRID
EXIT GRID
2.0
d_{ext}
1.5
d_{acc}
1.5
2.5
2.0
4.1
3.5
4.5
3.5
4.0
4.0
I_{dec}
V_{dec}
0-40kV
0-4 A
I_p
I_g
V_{ext}
0-35 kV
0-44 A
V_{acc}
0-50 kV
0-40 A
I_{acc}
ALL DIMENSIONS IN mm

Figure 4-13

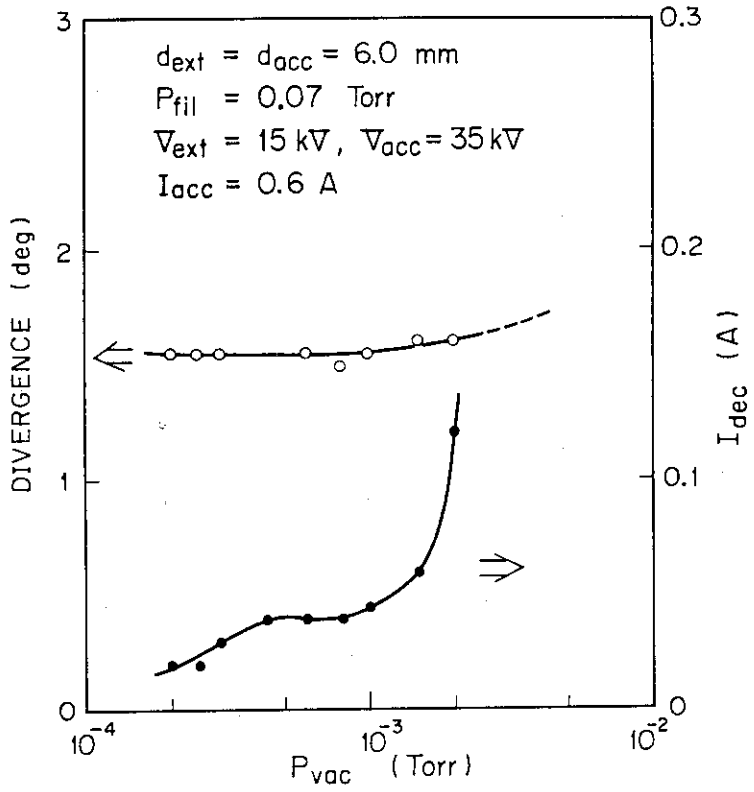

Figure 4-14

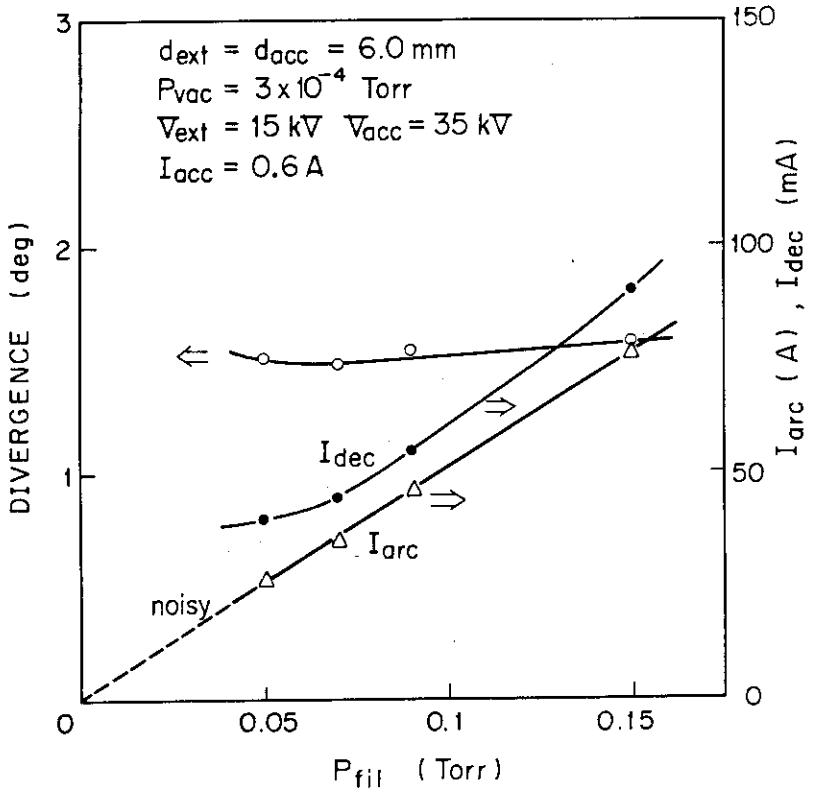

Figure 4-15

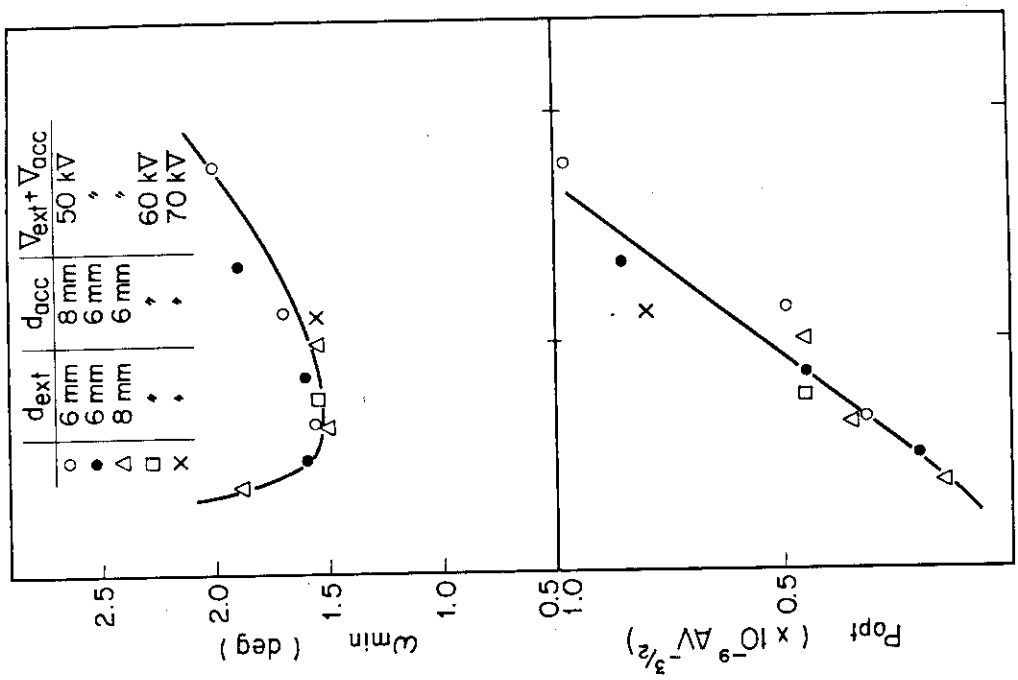

Figure 4-17

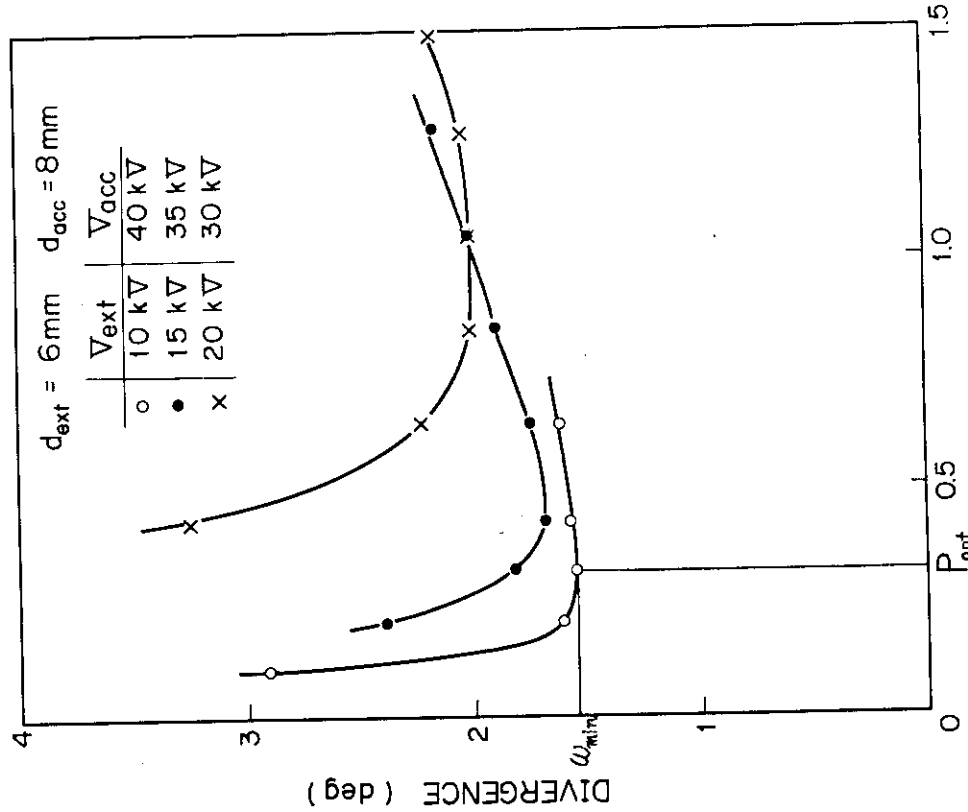

Figure 4-16

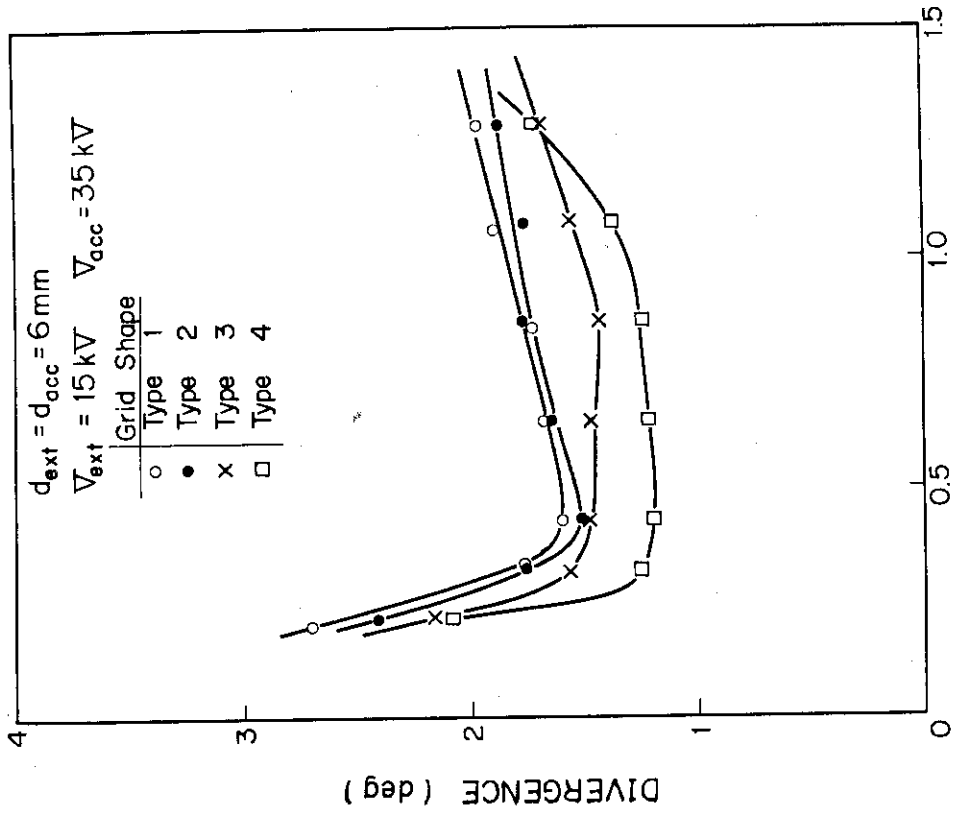

Figure 4-19

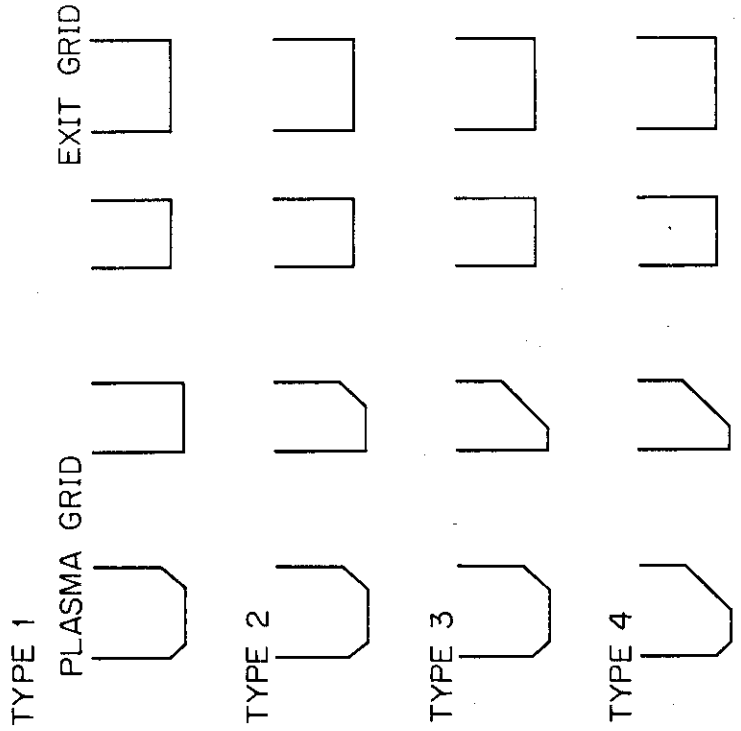

TYPES OF APERTURE SHAPE

Figure 4-18

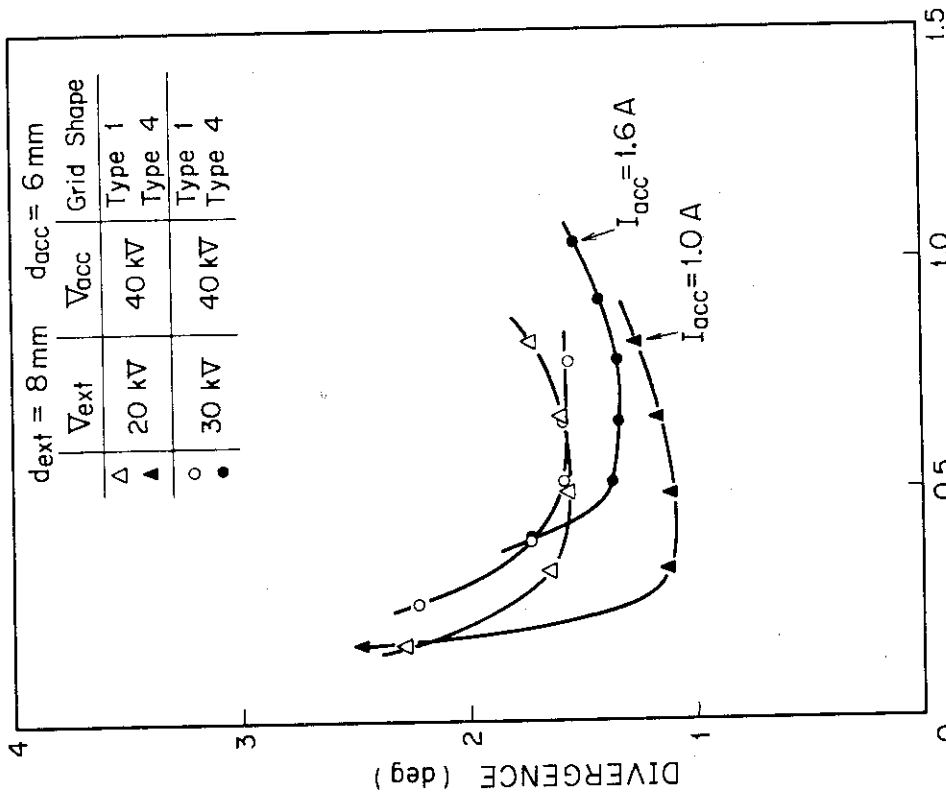

Figure 4-21

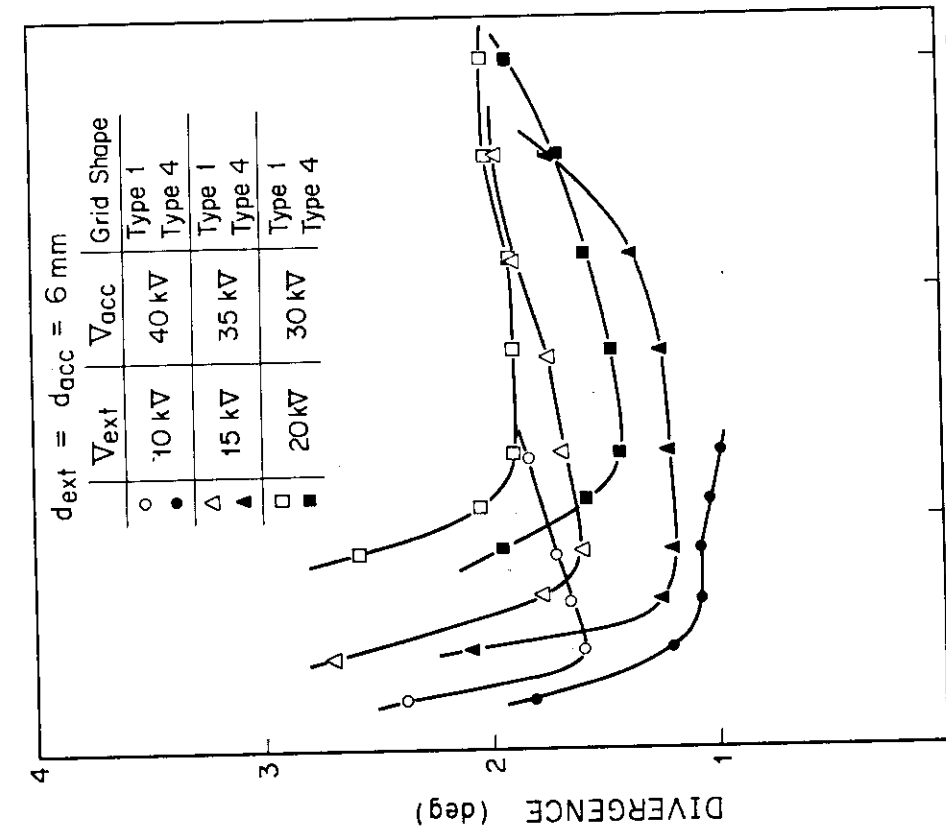

Figure 4-20

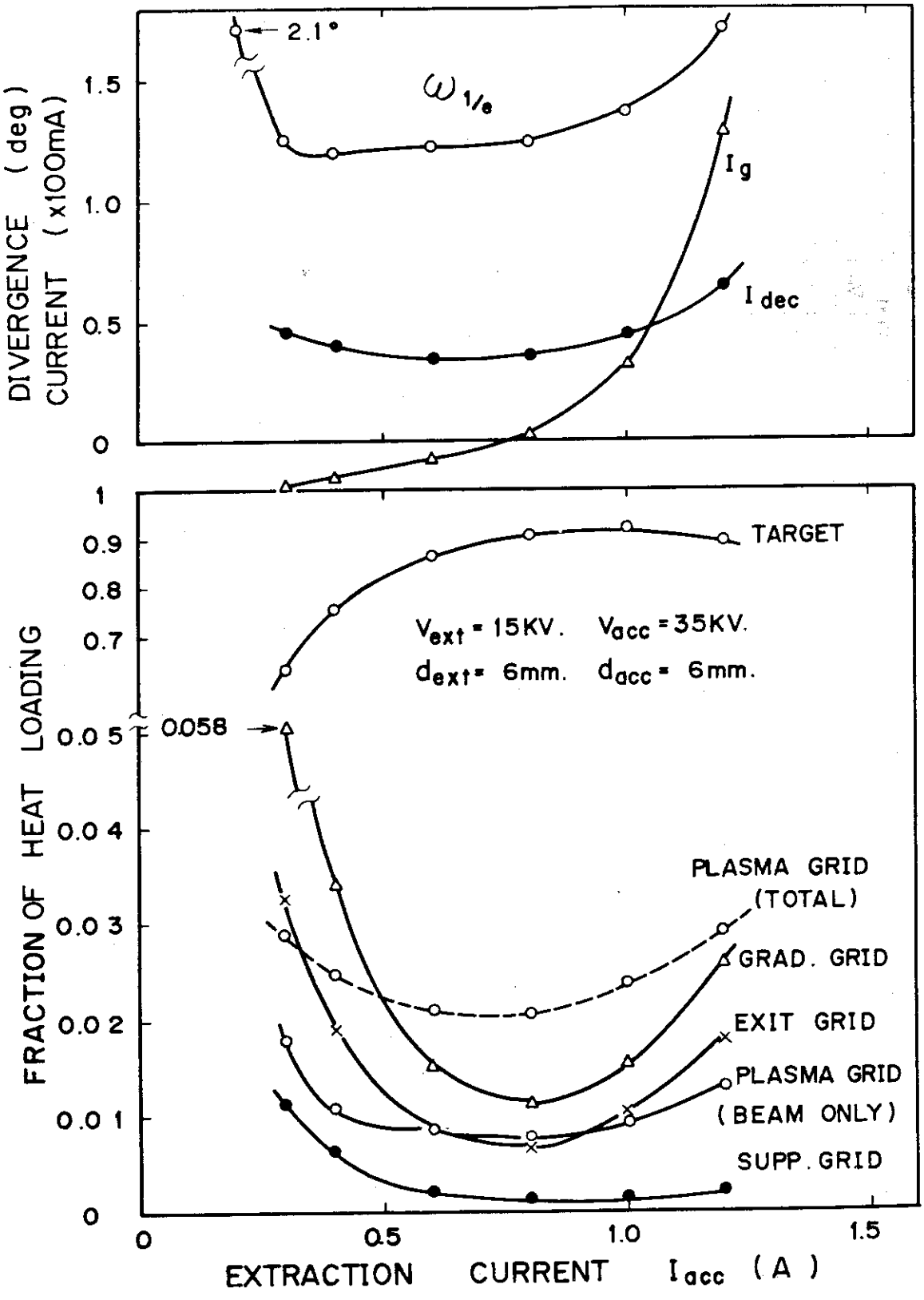
DIVERGENCE (deg)
CURRENT (x100mA)
2.1°
$\omega_{1/e}$
I_g
I_{dec}
FRACTION OF HEAT LOADING
TARGET
V_{ext} = 15KV. V_{acc} = 35KV.
d_{ext} = 6mm. d_{acc} = 6mm.
0.058
PLASMA GRID (TOTAL)
GRAD. GRID
EXIT GRID
PLASMA GRID (BEAM ONLY)
SUPP. GRID
EXTRACTION CURRENT I_{acc} (A)

Figure 4-22

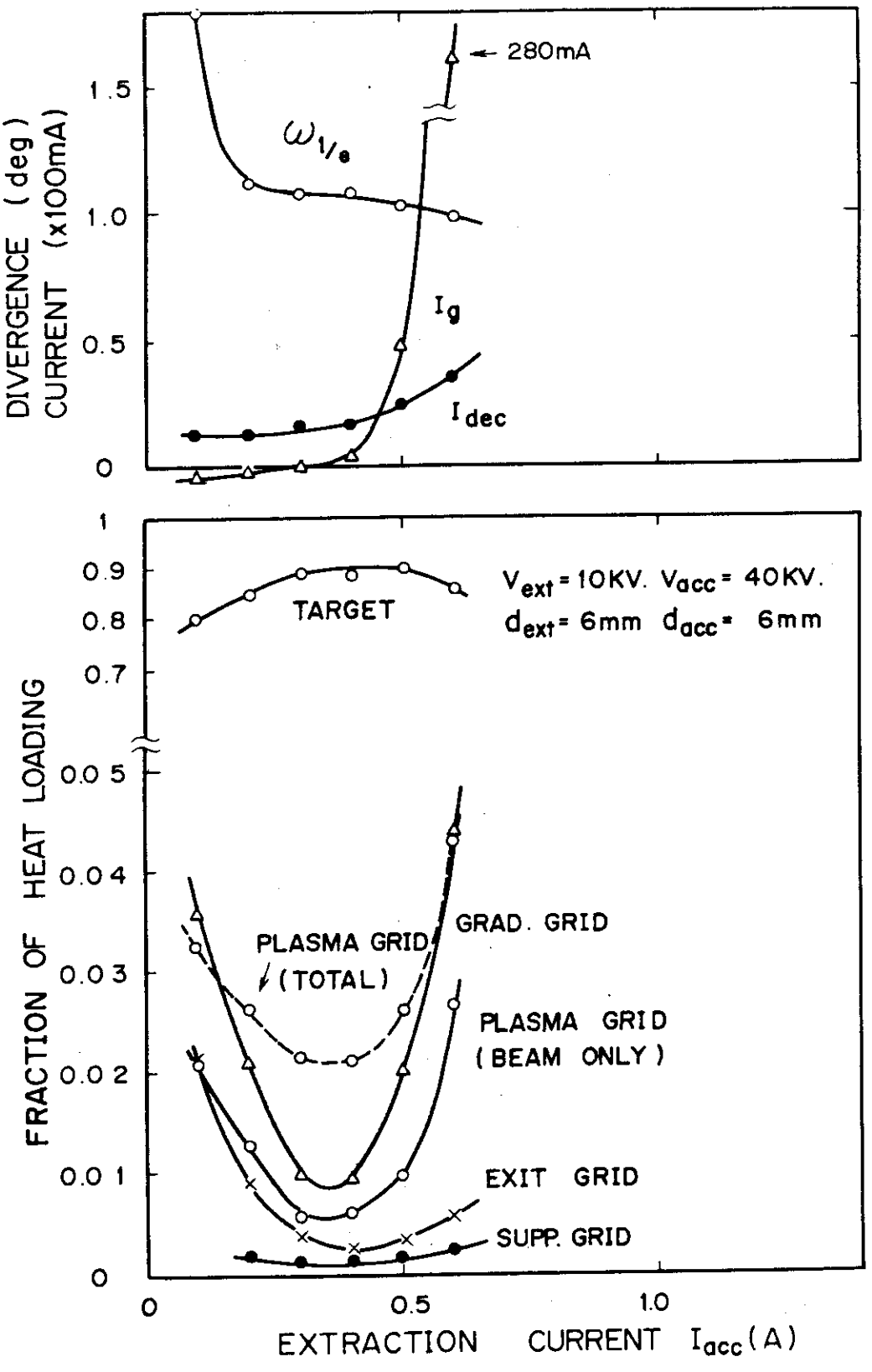
DIVERGENCE (deg)
CURRENT (x100mA)
1.5
1.0
0.5
0
280mA
$\omega_{1/e}$
I_g
I_{dec}
FRACTION OF HEAT LOADING
1
0.9
0.8
0.7
0.05
0.04
0.03
0.02
0.01
0
TARGET
V_{ext} = 10KV. V_{acc} = 40KV.
d_{ext} = 6mm d_{acc} = 6mm
PLASMA GRID
(TOTAL)
GRAD. GRID
PLASMA GRID
(BEAM ONLY)
EXIT GRID
SUPP. GRID
0
0.5
1.0
EXTRACTION CURRENT I_{acc}(A)

Figure 4-23

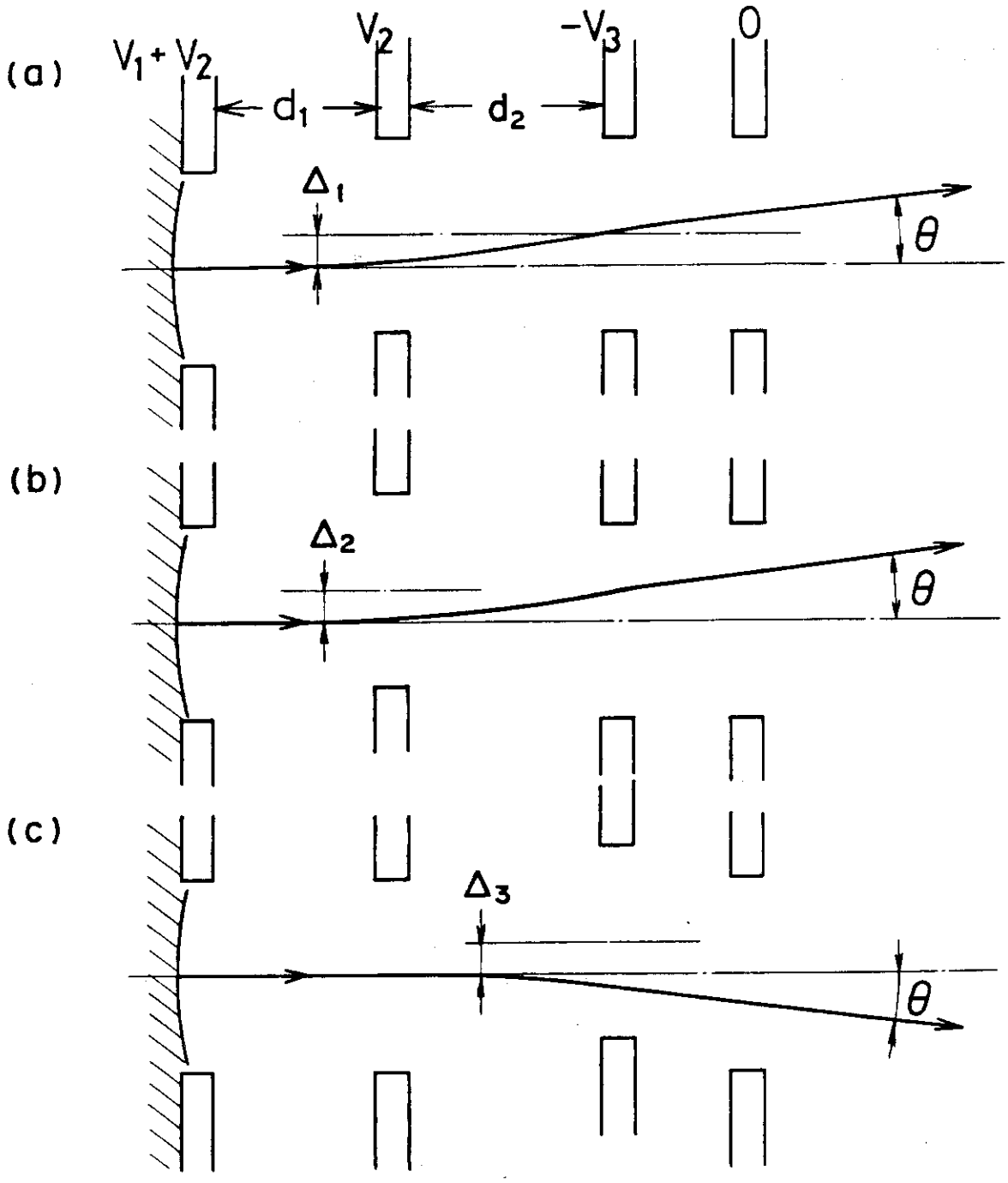

Figure 5-1

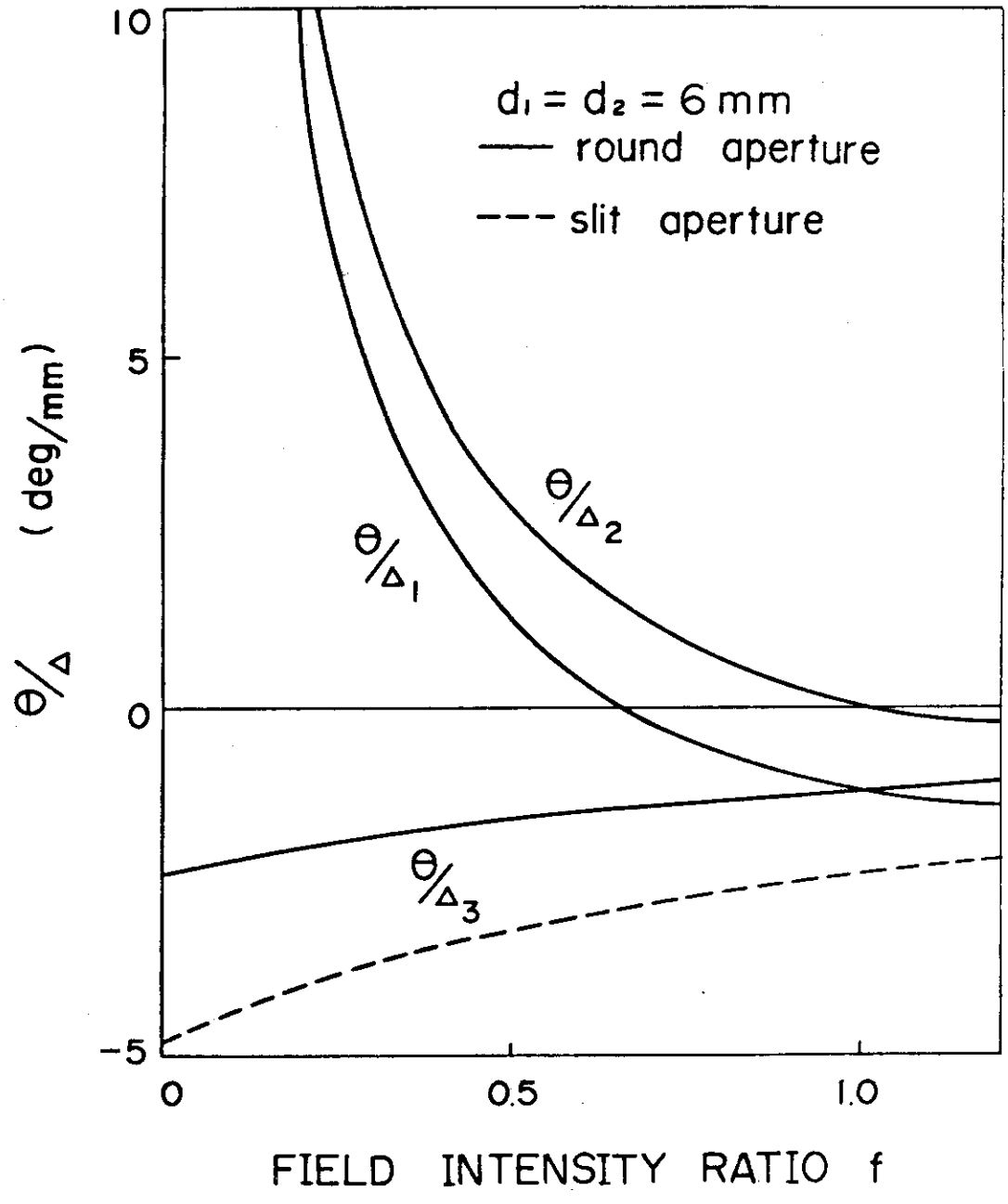
10
5
0
-5
0
0.5
1.0
θ/Δ (deg/mm)
FIELD INTENSITY RATIO f
d₁ = d₂ = 6 mm
round aperture
slit aperture
θ/Δ₁
θ/Δ₂
θ/Δ₃

Figure 5-2